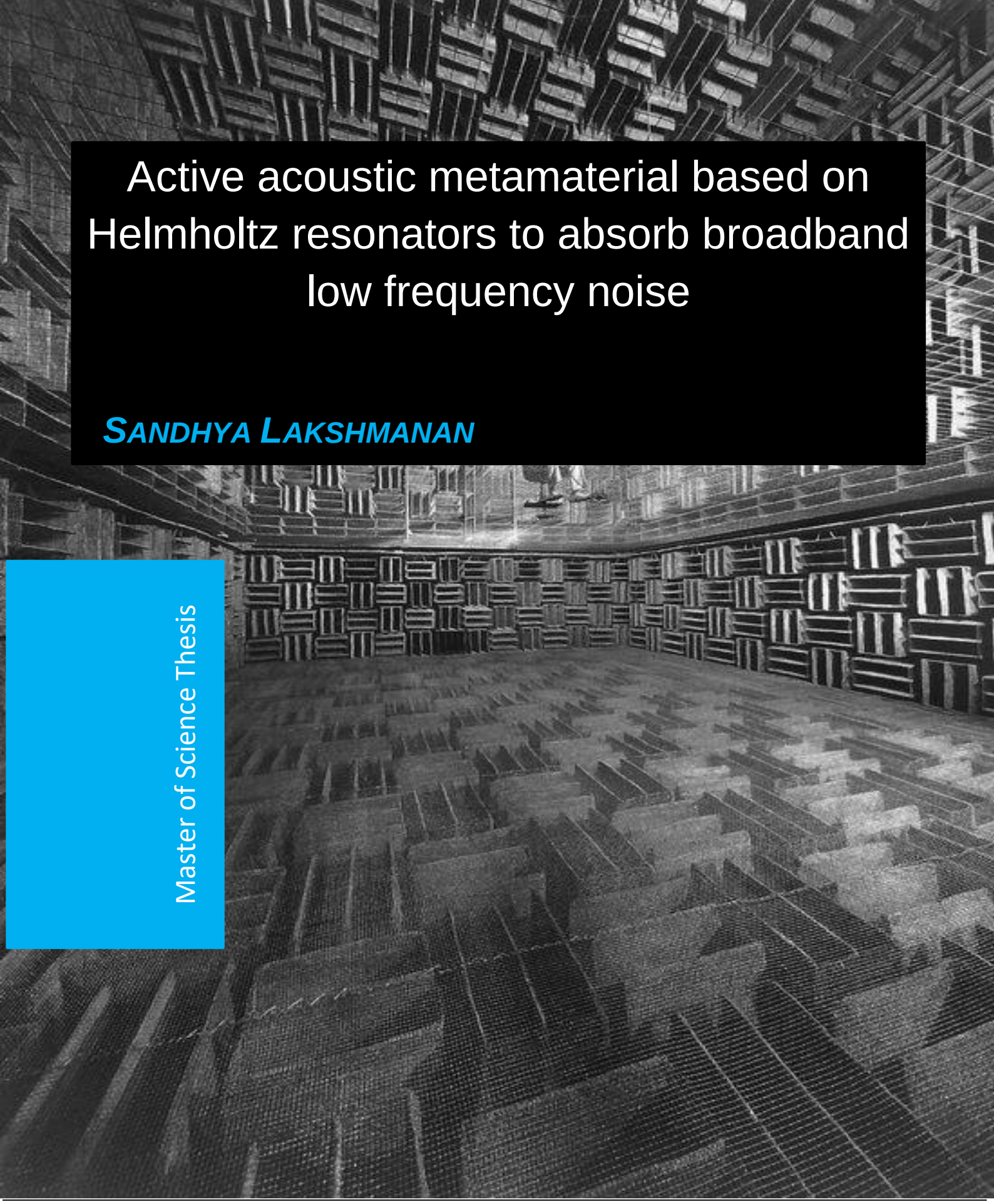

Active acoustic metamaterial based on Helmholtz resonators to absorb broadband low frequency noise

SANDHYA LAKSHMANAN

Master of Science Thesis

TU Delft

Novel Aerospace Materials

This page is intentionally left blank.

Active acoustic metamaterial based on Helmholtz resonators to absorb broadband low frequency noise

Thesis report

by

Sandhya P Lakshmanan

in partial fulfilment of the requirements for the degree of

Master of Science

in Aerospace Engineering

at the Delft University of Technology,

to be defended publicly on Wednesday October 24, 2018 at 09:00 AM.

Student number: 4612906

Thesis committee:		
	Prof. Dr. Ir. S. van der Zwaag,	TU Delft, Professor, NovAM, Chairholder of NovAM
	Dr. R. Hedayati	TU Delft, Post-doctoral researcher, NovAM Thesis supervisor
	Dr. D. Ragni	TU Delft, Assistant Professor External member
	Dr. Ir. J. Sinke	TU Delft, Assistant Professor External member

TU Delft

This page is intentionally left blank.

Acknowledgment

First and foremost, I would like to thank my thesis supervisor Dr. Reza Hedayati for his continuous support throughout the timeline of the project. The successful completion of the project would not have been possible without his support and guidance at every step. His technical expertise, criticism and encouragement helped me achieve the project goals.

I also thank Prof. Sybrand van der Zwaag for his guidance in helping me with my research by providing many practical suggestions that got this project going. It also helped me explore new possibilities in making the system work with minimal effort.

I would like to thanks Dr. Daniele Ragni, who provided his insight and guidance throughout my project. He was always available to answer any related queries and provided many clarifications regarding the applications of my thesis. Since working with acoustic structures was a new field of experience for me, his pointers and suggestions made it easier to explore the concepts of the field.

I would also like to thank Ing. Berthil Grashof who gave his full support in the DASML laboratory. His timely help and expertise in practical applications helped me a lot with my experimental setup and actuation systems for my project. In addition, I would like to thank Shanta, whose ever-smiling face brought in me a sense of encouragement every day. She has also been a great helping hand in all the administrative work and helped me through my project.

Furthermore, I would like to extend my sincere thanks to Ravi Tej, who was my big pillar of support throughout the course of my thesis and my study at TU Delft. His constant help with the analyses and the experiments is much appreciated. I also like to thank all the members of NovAM who have supported me throughout my course of study. Finally, I thank my parents who have always supported my decisions and were always by my side through everything.

This page is intentionally left blank.

Abstract

Metamaterials are a new class of materials that have properties that cannot be found in nature. Though these artificially engineered structures have not been prominently used in many applications, they have been theoretically studied to have a variety of applications in many sectors. Acoustic metamaterials have the capability of manipulating sound waves in order to achieve the required unique properties.

The aim of the project is to design an active acoustic metamaterial consisting of an array of Helmholtz resonators to assist in reduction of noise levels in aerospace applications using the method of 3D printing.

This project presents an active Helmholtz resonator based design that can attenuate a broadband range of targeted frequencies in the low-frequency regime. To this end, a passive metamaterial consisting of an array of Helmholtz resonator unit cells, with a single varying design variable, is designed and tested to establish the effectiveness and region of performance. The selected design variable for change is identified through the frequency response for each parameter of the Helmholtz resonance equation, to achieve a broadband frequency range of the metamaterial. An active model of this design is then fabricated and tested. Two actuation mechanisms are presented for this design. The resulting acoustic systems are capable of providing an attenuation of up to 20 dB, for an open system, and up to 35 dB, for a closed system, at frequencies between 150 Hz and 500 Hz. Unlike most other studies conducted, this active acoustic design is capable of attenuating isolated frequencies as well as multiple frequencies simultaneously. The added control that is achieved through the incorporation of the electric linear motor based actuation allows for the advantage of accurate frequency targeting along with the base attenuation levels of the passive resonant acoustic metamaterial.

This page is intentionally left blank.

Table of Contents

List of Figures

List of Tables

List of Abbreviations

A	Area of the neck
Al_2O_3	Aluminium Oxide
AM	Additive manufacturing
c	Speed of sound
f	Resonant frequency
FDM	Fused Deposition Modelling
L	Length of the neck
PLA	Poly lactic acid
SLA	Stereo lithography
SLS	Selective Laser Sintering
SPL	Sound pressure level
SRR	Split ring resonator
V	Volume of the cavity
VO2	Vanadium Dioxide

1

Introduction

A metamaterial is an artificially engineered material that has properties that are not usually found in nature. Even though there is no exact definition for this class of materials, they exhibit unique physical properties in a macroscopic level, such as a negative electrical permittivity, negative magnetic permeability, negative Poisson's ratio, negative bulk modulus, etc. Though metamaterials have not been prominently used in many applications, they have been theoretically studied to have a variety of applications in many sectors. These materials are found to acquire their unique properties from their design and structure, which gives them an inherent advantage over other classes of materials. These unique properties originating from structural arrangements were first noticed by Russian scientist Victor Veselago [1] in 1968. But since the observation that change in unit cell structures can result in macroscopic changes was not accepted and encouraged, the concept of metamaterials was dormant until another researcher, John Pendry [2], observed that a certain material's property of radiation absorption came from the physical structure of the fibers and not from the molecular structure. Since then, metamaterials have been vastly researched upon for their uses in fields like aerospace, optics, communications, which demand very specific properties in their structures. A lot of reports and papers have been published explaining experimental and theoretical work that proves the existence of certain properties that are unique to these type of materials.

1.1 Types of metamaterials

A broad classification of metamaterials can be obtained based on their responses to different stimuli. These stimuli include electromagnetic, mechanical and acoustic signals. Considering the appropriate responses to the input signals, the metamaterials are called electromagnetic, mechanical/elastic and acoustic metamaterials correspondingly.

Electromagnetic metamaterials, the first type of metamaterials discovered, are characterized by artificially created electromagnetic structures that respond to electromagnetic wave signals interacting with the structures. The element interactions of these structures can be used to form electric and magnetic responses and control light matter interactions. The unique responses to electromagnetic waves range from negative refractive index to applications like super lensing and cloaking. These responses can be altered according to the requirements by altering the geometry of the metamaterials rather than the chemical composition. Based on their abilities of operation for different frequency regimes, they can also be further classified as terahertz, plasmonic and tunable metamaterials. The application sector of electromagnetic metamaterials is wide considering significant advancements in non-destructive evaluations, electromagnetic cloaking, optics and communication, electromagnetic wave absorbance, etc. An example of an electromagnetic metamaterial is a structure with gold split ring resonators designed by Driscoll et al [3], that was able to induce magnetic permittivity in a non-magnetic material, thus creating an artificially magnetic material at high frequencies. In addition, introduction of vanadium dioxide (VO_2) in the material led to a temperature

controlled tuning of the permittivity at desired frequencies. Figure 1a shows the structure of the Split ring resonator and Figure 1b shows the permittivity peak shift corresponding to different temperatures.

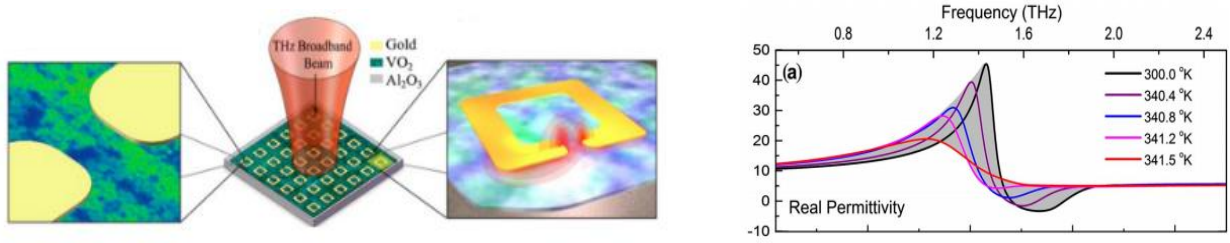

(a) **(b)**

Figure 1: (a) Schematic of the electromagnetic metamaterial with Vanadium oxide coated in between the gold SRR (b) Experimental measurement of permittivity of the metamaterial for different temperatures showing shift in frequencies [3]

Mechanical metamaterials, the next type, also called elastic metamaterials get their unique properties from the topology of their physical structure in response to a mechanical force [4, 5]. Some of these materials are made of small meta atoms, which have the property of adjusting the adjacent atoms to yield collective properties of the structures, which yield shape-morphing abilities. This has led to the design of auxetic structures that have unusual properties like negative Poisson's ratio which essentially implies that unlike the usual property of other materials, these special type of metamaterials contracts in the transverse direction under a compressive force as shown in Figure 2 [6].

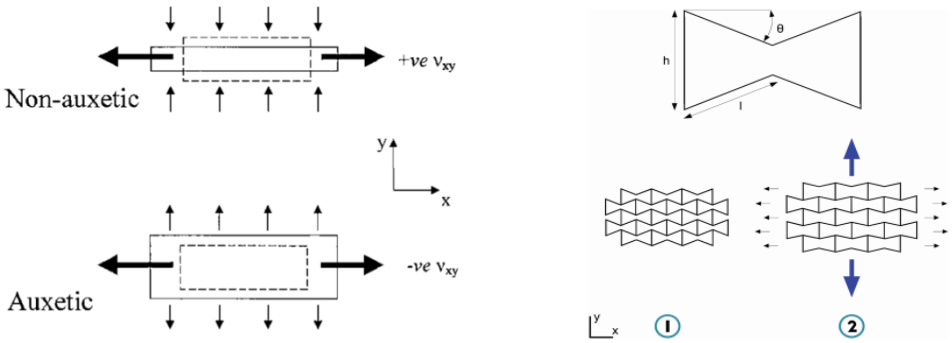

(a) **(b)**

Figure 2: (a) Auxetic and non-auxetic behavior of materials in response to an axial force (b) Deformation of a re-entrant bow tie structure [6]

The third broad classification of metamaterial accounts to acoustic metamaterials. These materials exhibit the property of controlling and manipulating sound waves in different mediums using their structural arrangements. This type of wave controlling happens due to small non-homogeneities that produce macroscopic changes. Based on the design of their structure, acoustic metamaterials can be

of different types namely, membrane type, plate type, space coiling, ultrasonic etc. Acoustic metamaterials are widely preferred in applications where noise reduction is of significance. In this aspect, the concept of Helmholtz resonance provides a convenient solution. Due to its relatively simplistic design and working principle, studies are being conducted on incorporating Helmholtz resonators in metamaterials for effective noise attenuation. These artificially formed acoustic structures can be passive for a fixed range of frequencies or dimensionally modulated to create an active system targeting multiple frequencies. An example of an active acoustic system which has Helmholtz resonators incorporated in the structure was designed by Simon et al [7] in which damping was achieved by altering the opening diameter of the resonator by an iris opening mechanism. An acoustic mesh was also placed to control the damping ratio for larger opening diameters. The damping obtained for different opening diameters are shown in Figure 3b.

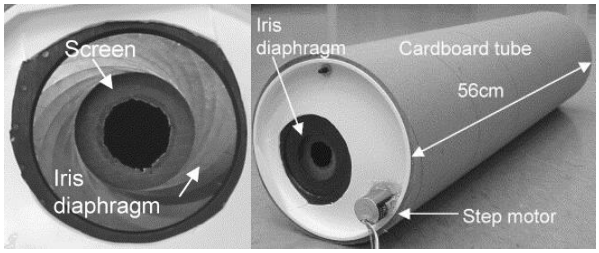

(a)

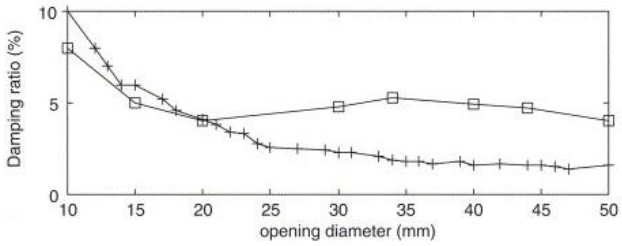

(b)

Figure 3: (a) Structure of the adaptive system with adjustable neck openings (b) Damping ratios for different frequencies [7]

1.2 Project goal and hypotheses

The main objective of this thesis is to design an active acoustic metamaterial to adaptively control noise signals of different frequencies. The use of Helmholtz resonators is seen as the most convenient and tunable means to achieve this end. As the theoretical resonant frequency targeted by the resonator is dependent on the dimensions of the two sections of the resonator, it is hypothesized that altering one or more of these dimensions allows for active control of various noise signals. Additionally, the use of multiple resonators with varying internal dimensions is theorized to passively be capable of performing effectively over a range of frequencies. The proposed method of realizing this hypothesis is to alter one dimension of the resonators, and verify the effect on noise attenuating capabilities.

In order to achieve this goal, the project is divided into two major phases. The first phase is the design of a passive prototype that targets a broadband frequency range. This passive model is expected to define the range of operation for the active model.

Based on the performance of the passive model and the frequency range defined, the actuation of the active model is chosen such that the most significant design parameter is varied to target specific frequencies in the broadband range.

This is a step towards the ultimate goal of being able to effectively identify dominant frequencies and reduce their corresponding noise levels through a fully adaptive system that varies more than one parameter to achieve a better frequency range as well as an efficient noise attenuation performance.

In this report, the next chapter presents an extensive state of the art background study to aid in the design and experimentation of the model. In the following chapter, the experimental methodologies and the technical description of the equipment used for fabrication are established. Following this, the results of the passive model and by extension, the conversion of passive into active model is discussed after which the future possibilities and recommendation for an improved metamaterial are elaborated.

2

State of the art literature study

In the past years, many numerical and experimental studies have been conducted on this concept of acoustic metamaterials pertaining to many applications. Though this thesis is based on the design of the acoustic structure for the purpose of noise reduction, various types of acoustic metamaterials have been explored to understand their working and advantages over existing materials corresponding to each application. In this section, a literature study encompassing the publications most relevant to this project is presented.

2.1 Acoustic metamaterials

As introduced in the previous section, acoustic metamaterials derive their unique properties by manipulating sound waves by means of their structural arrangements. Initial research on acoustic metamaterials started when Liu et al [8] fabricated an 8×8×8 sonic crystal made of spherical lead cores coated with silicone rubber as shown in Figure 4a. The transmission level was measured as a function of frequency showed that resonance induced negative values of elastic constants for a material could be achieved.

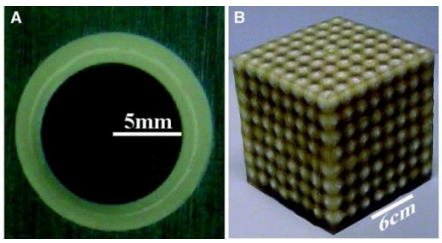

Figure 4: Cross-section of a unit spherical lead cell coated with silicone rubber and the lattice structure of the sonic crystal with the array of spherical crystals [8]

This was followed by Smith et al [9] who combined a split ring resonator in a sonic structure to design an acoustic metamaterial that was able to induce negative values of magnetic permeability thus paving the way to the design of the first double negative acoustic metamaterial by Li et al [10]. This metamaterial showed both negative density and negative bulk modulus simultaneously making it analogous to Veselago's electromagnetic metamaterial.

Based on the response of the acoustic metamaterials at certain resonant frequencies, the properties they are aimed at manipulating and their structural arrangements, they can be further classified into membrane and plate type, double negative and space coiling acoustic metamaterials.

2.1.1 Membrane and plate type acoustic metamaterials

The membrane type acoustic metamaterials are known for their negative dynamic mass density characteristics, which by stacking at different frequencies gives a broad operational band spectrum

[11, 12]. Effective negative mass density can be seen when the dynamic mass of the system tends to a value less than zero [13]. This can be realized when the force acting on the mass and its acceleration are out of phase to each other. These materials are typically known to operate in frequencies ranging from 50 to 2000Hz. Apart from their characteristic negative mass density [14], it has also been experimentally found that these materials have the ability to induce negative values of bulk modulus. These type of materials inducing simultaneously negative values of density and bulk modulus are termed as double negative acoustic metamaterials [10, 15]. Such a double negative membrane type metamaterial was demonstrated by Yang et al [12] who designed a metamaterial with coupled membranes [16] (as shown in Figure 5a) that was able to generate tunable resonance in a broadband frequency range. Furthermore, membrane type metamaterials are also used for lightweight structures that are applicable for noise attenuation of low frequency noise signals. [17].

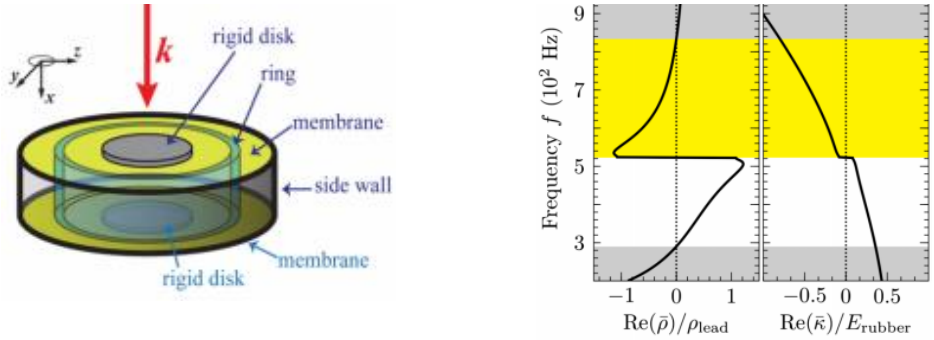

(a) **(b)**

Figure 5: (a) Schematic of the metamaterial with coupled membranes (b) Frequency plots showing negative dynamic mass density and bulk modulus [12]

Plate type acoustic metamaterials are similar in construction to the membrane type but constitutes of stacked rigid plates instead of membranes. They provide much more rigidity than the membrane type metamaterials, which use rubber membranes. For attenuating low frequency noise, theoretically the thickness of the plate type material should be comparable to the wavelength of the sound. However, plate type metamaterials are more rigid and thick as compared to membrane type. This poses a constraint on the mass and volume of the system. Hence, to overcome this, modifications are made to the structure of the plate type metamaterials to enhance their low frequency attenuation performance [18]. For example, Assouar et al [19] proposed a design of a robust plate type metamaterial that could attenuate low frequency noise at a resonant frequency range of 650 to 3500 Hz. The metamaterial structure consisted of composite stubs arranged on a thin aluminium plate which when introduced to a noise source, reduced the level of transmission significantly across the stubs as shown in Figure 6a.

The main advantage of both membrane and plate type acoustic metamaterials is that they are usually lightweight structures. This is significantly important in aircraft application where the engine noise poses a major problem. In such scenarios, these type of light structures that target low frequencies are highly efficient.

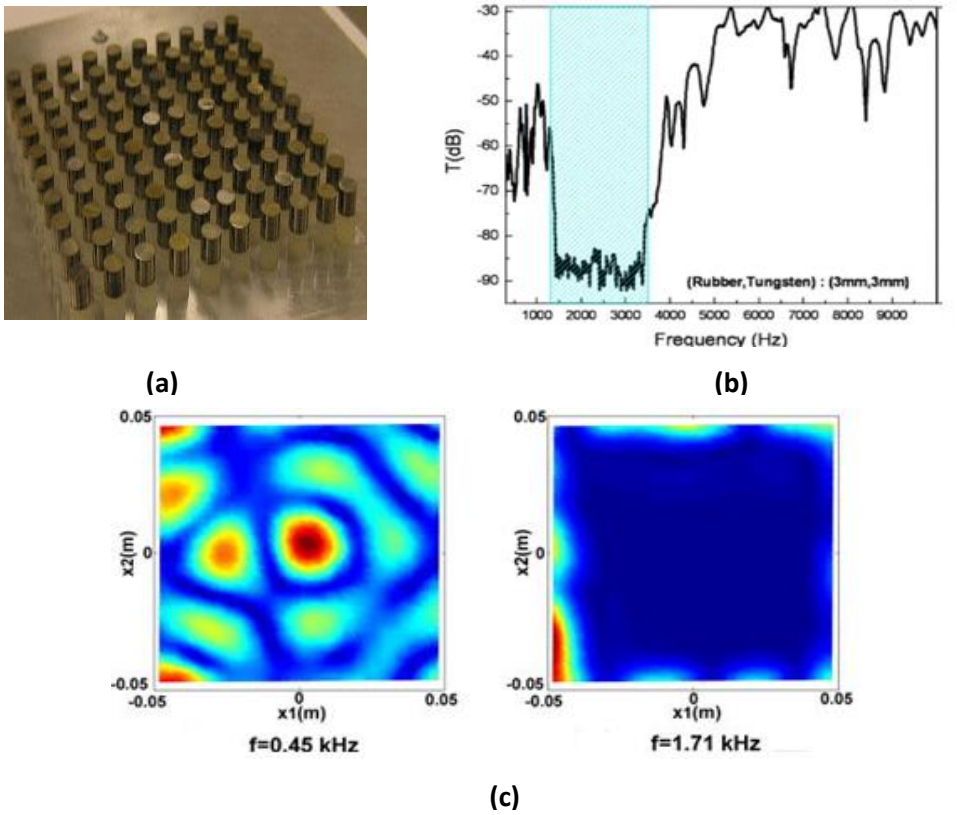

Figure 6: (a) Picture of the fabricated plate type acoustic metamaterial with composite stubs embedded in the aluminium plate (b) Transmission characteristics and bandgap determined from the measurements at different frequencies (c) Sound transmission characteristics for frequencies below(Left) and inside(Right) the Bandgap [19]

2.1.2 Acoustic space coiling metastructures

The concept of space coiling metastructures was first proposed by Liang and Li [20] who demonstrated the performance enhancement of a 2D acoustic metamaterial using curled perforations in space. Acoustic waves, being scalar in nature, allow for the use of coiled subwavelength channels to increase the effective path length in a confined space when the cut-off frequency is absent as shown in Figure 7. This increase in path length leads to a phase shift of the wave with respect to the incident wave thus resulting in a high refractive index [21]. In a system where part of the acoustic waves passes through the coiled channel, the refracted wave introduces an impedance on the unrefracted wave, reducing the amplitude and intensity of the effective output [22, 23]. Space coiling mechanisms have also been used to achieve double negativity in 2D and 3D structures acoustic structures which has led to easy tunability of wavelengths by adjusting the number of curls on the channels of wave propagation [24].

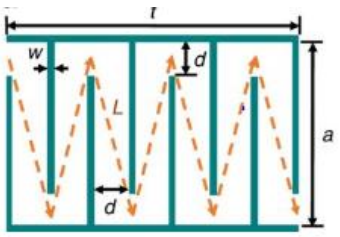

Figure 7: Space coiling structure in a unit cell and the effective increase in the path length of the acoustic wave [22]

2.2 Applications of acoustic metamaterials

2.2.1 Acoustic cloaking

An acoustic cloak is a material, which when placed over an object has the ability to manipulate the acoustic waves around the object, thus rendering the object acoustically invisible. Cloaking is done by deforming the region such that mapping can be done everywhere around the cloak except at a single point which points to the cloak's inner boundary [25, 26]. Thus it is made sure that the properties of the inner boundary namely density and modulus, mimic the outside properties of the region. Any transformation made to an elastic region will have an anisotropic aspect to it and hence anisotropy is inherent in these type of transformations. There have been reports of acoustic cloaks proposed out of coordinate transformations for broadband noise in a wide frequency range of 50-60 kHz [27]. Acoustic metamaterials were first used in an acoustic cloak designed by Kan et al [28], who used an array of perforated plates that contained subwavelength inclusions thus making an acoustic structure without any resonating components. The 3D printed cloak kept over an object and the structure of a unit cell of the metamaterial are shown in Figure 8a.

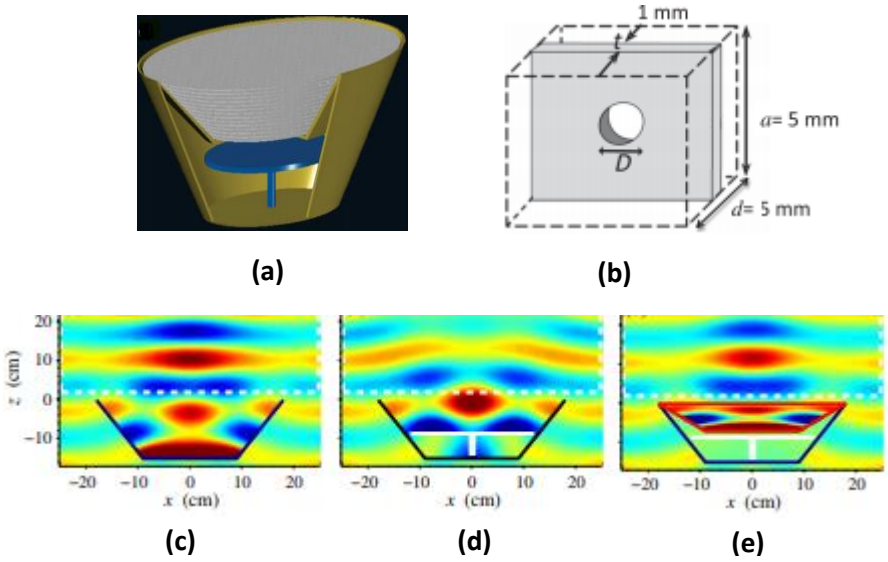

Figure 8: (a) cross section of the setup with an object and the metamaterial cloak (b) unit cell of the metamaterial ; Pressure field from simulations for (c) without the object (d) with the object (e) with the object and the cloak [28]

2.2.2 Noise attenuation

The application of noise attenuation has always been one of the significant issues in many sectors. There have been many proposed methods of noise reduction using various materials and structures. The discovery of acoustic metamaterials has paved a way to provide significant improvement in this demanding area of application in fields like automotive and aviation. For instance, a lightweight acoustic metamaterial suited for aviation designs where weight reduction is important was proposed by Sui et al [29]. This is a challenge, as theoretically, the amount of sound transmission is known to be inversely proportional to the thickness and density of the material. To overcome this limitation, a

honeycomb design was proposed, that yielded in a lightweight soundproof structure. This structure was experimentally proven to attenuate about 15 dB of noise. Furthermore, a numerical demonstration of a vibro-acoustic metamaterial which had a resonant structure on a hollow core sandwich structure was done by Claeys et al [30] to investigate sensitive parameters in the design of acoustic metamaterials. Similar numerical work have also been shown by other researchers to investigate the mass density and topology optimization of such acoustic metamaterials [31]. Moreover, many other experimental and theoretical works have been done in this field combining the concept of Helmholtz resonance in the design of acoustic metamaterials which is explained in detailed in the next section. An overview of the publications referred in this study of acoustic metamaterials is shown in Table 1.

Table 1: Overview of publications based on acoustic metamaterials

Acoustic Metamaterials	References
Membrane and plate type Acoustic metamaterials	[10-19]
Acoustic Space-Coiling metastructures	[20-24]
Acoustic Cloaking	[25-28]
Noise reduction	[29-31]

2.3 Helmholtz resonance

Helmholtz resonance is a phenomenon where resonance is created when air enters an open hole or a neck that leads into a bigger cavity. Common examples include neck of an empty bottle, guitars, ocarinas, etc. The basic principle is explained by considering the air inside a Helmholtz resonator as a spring-mass system with the air at the neck representing the mass and the air inside the cavity working as a spring. As shown in Figure 9, when air is blown over the top of a Helmholtz resonator, the air at the neck of the cavity is compressed. This leads to an increase in the pressure inside the cavity, which tends to restore it back to the original volume. When this process almost comes to an equilibrium state with a restoring force $F = -k\Delta x$ the air is pushed from inside to the outside of the cavity by certain momentum. This leads to a decrease in the pressure of air inside the cavity, which results in the air being sucked back inside. This phenomenon keeps repeating thereby making the air inside springy, thus vibrating the mass at the neck of the cavity [32].

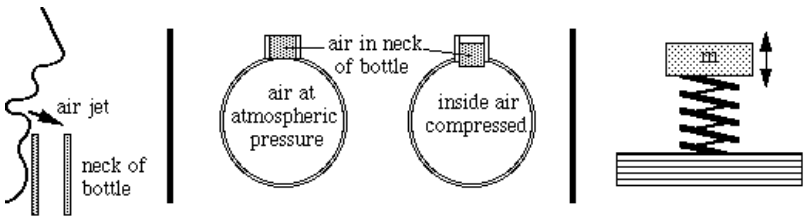

Figure 9: Phenomenon of Helmholtz resonance where air inside the cavity is modelled as a spring mass system [32]

The above explained concept of Helmholtz resonance can be mathematically expressed by the Helmholtz equation that related the resonance frequency, the volume of the cavity, the length of the neck and the area of the neck as follows:

$$f = \frac{c}{2\pi}\sqrt{\frac{A}{VL}} \quad (1)$$

where,

c is the speed of sound

A is the cross-sectional area of the neck

V is the volume of air in the container and

L is the length of the neck

Due to its simplistic design and characterization, the incorporation of Helmholtz resonators into acoustic designs have been proven effective in both design and performance. There has been extensive research in this field of acoustics that has led to the design of acoustic metamaterials made of Helmholtz resonators to reduce noise transmission levels and increase the tunability of the acoustic system to required frequencies.

2.4 Application of Helmholtz principle in metamaterials

The application of Helmholtz resonance in acoustic metamaterials most commonly can be seen as the use of unit cell resonators that possess the basic structure described in section 2.3 and are capable of fixed frequency attenuation. This process of sound attenuation may be done by both passive and active designs. Passive designs target a selected range of frequencies that can be attenuated by a fixed resonator cavity [33]. According to the Helmholtz equation, a change in any one or all of the parameters brings about a change in the target resonant frequency. An example of a passive Helmholtz resonator based design is the model presented by Ding et al [34], who used split hollow spheres as Helmholtz resonators to prove that transmission losses can be achieved for different target frequencies by changing the neck diameter of the Helmholtz cavity as shown in Figure 10. The metamaterial was experimented with three different neck diameters (Sample A- 3mm, Sample B- 5mm and Sample C- 6mm) for which three transmission dips were observed. From this, a multiband acoustic metamaterial targeting an 800 Hz to 1600 Hz frequency range was modelled.

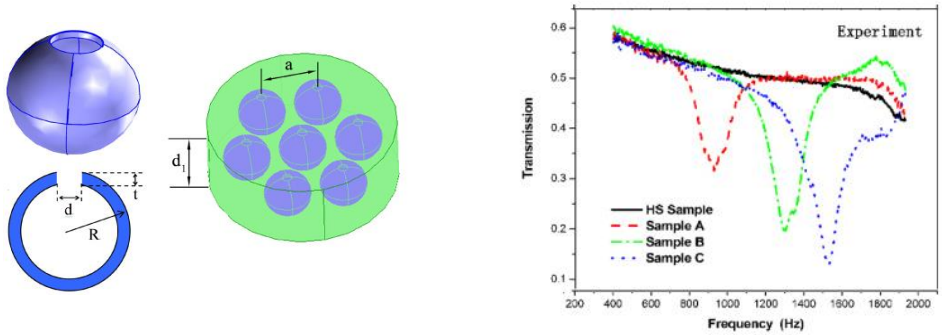

(a) **(b)**

Figure 10: (a) Schematic of the Split hollow sphere modelled as a Helmholtz resonator embedded periodically in a sponge matrix (b) Transmission of samples showing three different frequencies for 3 different neck diameters [34]

Similar passive structures have been designed and studied theoretically and experimentally by Wu et al [35], Zhao et al [36], Anwar et al [37], Ozar et al [38], etc. aimed at reducing noise transmission levels. Since the passive structures cater only to a fixed band, development of an active system that is capable of shifting the region of operation based on application requirements without preparation of separate structures for each frequency band would be a solution to the rising need of adaptive acoustics. Hence, active metamaterials where the dimensions of the resonators are changed adaptively by a mode of actuation are preferred.

In a Helmholtz resonator based active metamaterial design, there are three parameters that can be dimensionally altered: The volume of the cavity, the diameter of the neck and the length of the neck. In this section, some examples of active metamaterial designs are shown to investigate the effectiveness of each altering parameter. In addition, a comparison table summarizing the referred designs for this project is shown to aid the proposed design.

The easiest way to control the dimensions of the resonator for the active system would be to change the volume of the resonator cavity. Since this does not involve having actuations near the neck where the sound waves enter, it is easy to model without any disturbances in the measurement. One such model of an active metamaterial was designed by Birdsong and Radcliffe [39] who designed a noise control device based on semi-active Helmholtz resonators that was able to reduce transmission of noise when connected to an acoustic system like a duct or a pipe by actively changing the cavity volume by altering the depth of the resonator cavity. The frequency response measured shows that the system was configured to zero gain and maximum noise attenuation was achieved at the four main frequency peaks. Another tunable resonator design proposed by Bedout et al [40] that operated in the range of 65-150 Hz was able to achieve reduction in noise levels of about 29 dB adaptively by changing the volume of the resonator by blocking a section of the cavity by means of a rotary actuated moving wall as shown in Figure 11a. Self-tuning capabilities of the resonator system was demonstrated along with an open-loop tuning algorithm. Figure 11b shows the relation between the excitation frequency and noise level for the system with and without the self-tunable resonator.

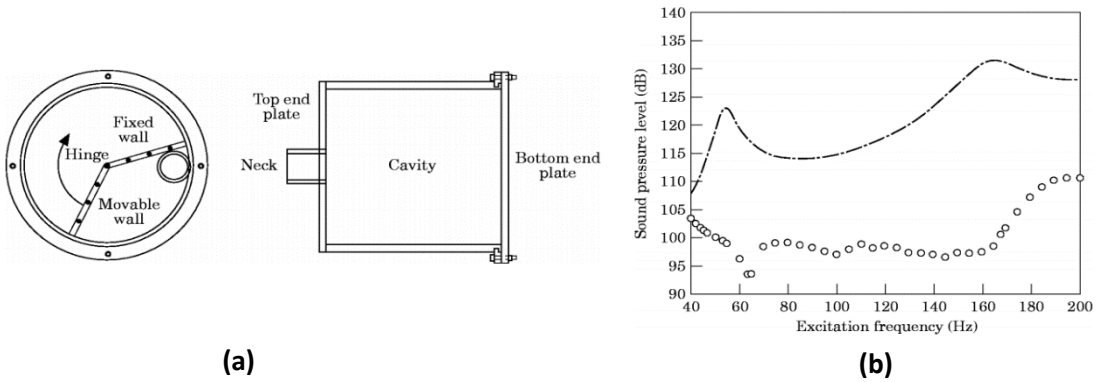

(a) **(b)**

Figure 11: (a) Structure of the resonator with the rotary actuated moving wall (b) Noise levels for various excitation frequencies without the tunable resonator (–·–) and with the tunable resonator (○) [40]

Another system presented by Kosuke et al [41] involved a two stage Helmholtz resonator that had auto-tuning control capabilities at around 3000 Hz. One stage was used for low frequency noise attenuation and the other for high frequencies. In addition, the decrease in the sound pressure for

designs with and without the resonators at a driving voltage of 130V are shown in Figure 12b from which the decrease in the output noise can be observed.

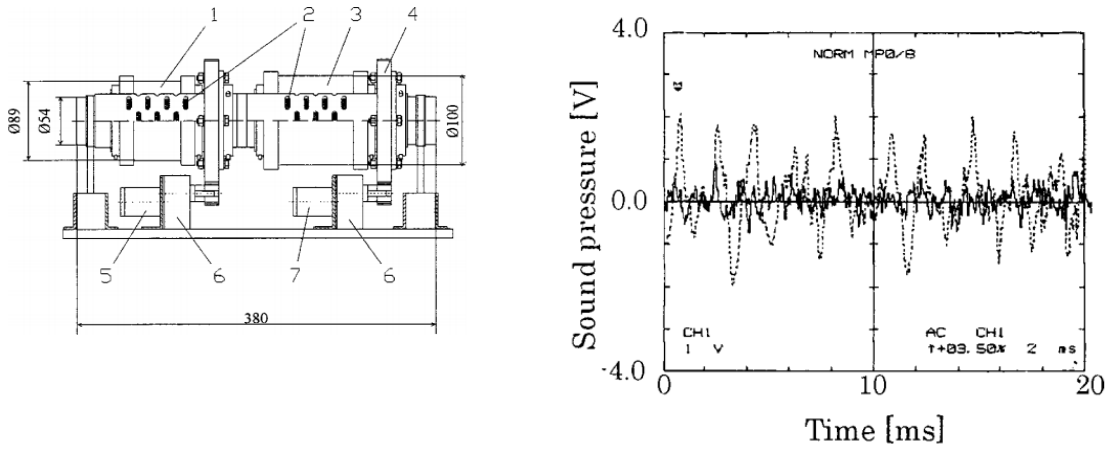

(a) **(b)**

Figure 12: (a) Structure of the Silencer with the two-stage resonator (Left) and cross section of a resonator (right) Here, 1,2,3 represents the Helmholtz resonators, 4 represents a gear and 5,6,7 represents the control motors (b) Sound pressure with (Black solid line) and without the silencer (dotted line) [41]

Moreover, the active metamaterial design of Cheer et al [42] also proved that by increasing the number of active resonators in the metamaterial model, the noise transmission level is found to decrease as shown in the plot in Figure 13. Furthermore, in Table 2, the different types of actuation mechanisms used for altering different dimensional parameters in the resonators aimed at reducing sound pressure levels are listed. The amount of sound attenuation achieved is also studied to evaluate the efficiency of each actuation technique.

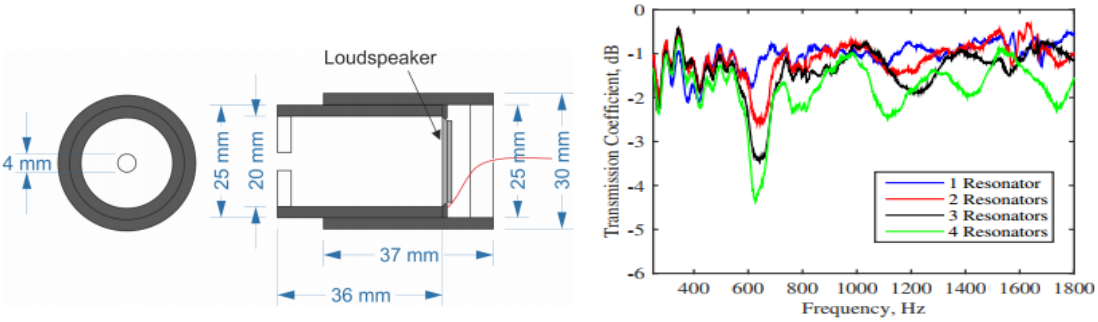

(a) **(b)**

Figure 13: : (a) Structure of the Helmholtz resonator used in the metamaterial (b) Transmission coefficients of the units with increasing number of active resonators [42]

Table 2: Comparison of Performance and Execution of Helmholtz Resonator Based Acoustic Metamaterials

Type of Volume Change (neck/cell)	Decrease in noise (dB)	Range of frequency (Hz)	Actuation Type	Range of Changing parameter	Type (Self-tuning, active, adjustable)	Publication
Cell Volume change	100%	80-170	Pneumatic	NA	Adjustable	[39]
Neck diameter	4.2 dB	75–115	Rotary actuated aperture	9-58 mm	Adjustable	[7]
Volume	29 dB	65-150	Rotary actuated walls	1491 cm^3-14093 cm^3	Self-tuning	[40]
Cavity Length	20 dB	-	Hydraulic	43-243 mm	Active	[43]
Internal Pressure		50-500 (Max – 160)	Electromagnetic diaphragm/ piezoelectric	NA	Active	[44]
Cavity length	18 dB	0-400 (max-226)	-	60-90 mm	Adjustable	[45]
Neck length	-	3-75	Hydraulic	39-60cm	Adjustable	[46]
Length of cavity	30 dB	80-140	Pneumatic	560 cm^3-940 cm^3 1.8-17 cm	Adjustable	[47]
Area of neck	25 dB	100-3000	Rotary	-	Self-tuning	[41]

Assessing the different possibilities of changing the dimensional parameters of the Helmholtz resonators to achieve attenuation, it is noticed that each of the cases presented previously in literature (Table 2) provide for the attenuation of a single instantaneous frequency, and involve a relatively complex mechanism of construction. The proposed design of the active acoustic metamaterial aims to combine the effects of an active resonator unit cell in a lattice structure, capable of attenuating multiple instantaneous frequencies, i.e., more than a single target frequency at the same time. In addition, the active and passive systems are designed such that the possibilities provided by 3D printing are taken advantage of.

3

Experimental methodologies

3.1 Metamaterial design

After an extensive literature study and comparison of some relevant metamaterial designs based on Helmholtz resonators, an active acoustic metamaterial with Helmholtz resonator unit cells is chosen as the metamaterial in consideration, to study the noise attenuation performance. To this end, a passive design is made in order to benchmark the limitations and performance expectations of the aimed design. In this section, first the models made for the experimental study are described in detail. The fabrication process and the experimental set up including the measurement techniques and equipment are also described afterwards.

3.1.1 Passive metamaterial

In order to evaluate the metamaterial performance parameter for the final active metamaterial, a passive metamaterial design targeting a fixed range of frequencies is proposed. From the Helmholtz resonance equation (Eq. (1)), the impact of each dimensional parameter on the frequency response is investigated leading to the conclusion that the frequency is mostly sensitive, in a low frequency regime, to a change in volume of the resonator cavity. The passive metamaterial is thus designed to cater to a range of approximately 150Hz to 500Hz, since this range of frequency contributes to a high loudness sensitivity in the aerospace industry and the attenuation of these frequencies is a requirement. The specific dimensions of each unit cell are derived from the fabrication limitations that set an upper bound to the width of the metamaterial. The constraints thus allowed for incorporating an array of 8x8 unit cells.

The unit cell of the metamaterial design is shown in Figure 15. The cross-section of the resonator is chosen to be a square for the simplicity of fabrication, while allowing a larger cross-sectional area of each unit cell. The base of the cavity is designed in the shape of a 'V' in order to avoid support structures during additive manufacturing as opposed to a flat base. The dimensions of the unit cells have been selected based on the resonant frequency range obtained from the Helmholtz resonance equation (Eq. (1)). The dimensions of the resonator and the metamaterial walls are listed in Table 3. Furthermore, the targeted design frequencies corresponding to each of the cavity lengths are shown in Table 4. The frequency and the cavity volumes are also plotted to determine the operational frequency range of the metamaterial (Figure 14).

Table 3: Dimensions of the resonators and the passive metamaterial walls

Parameter	Dimensions
Diameter of the neck	1.2 mm
Length of the neck	14 mm
Cross-section of the cavity	14×14 mm^2

Lengths of the cavities	8 – 42 mm
Area of the metamaterial wall	135×135 mm^2
Depth of the metamaterial wall	61 mm

Table 4: Resonant frequencies corresponding to depths of the resonator cavities

Cavity Depth [mm]	Cavity Volume [mm^3]	Resonant Frequency [Hz]
8	8.82E+02	522.4468656
10	1.27E+03	434.7020683
12	1.67E+03	380.1359313
14	2.06E+03	342.0217583
16	2.45E+03	313.4681194
18	2.84E+03	291.0478422
20	3.23E+03	272.8389772
22	3.63E+03	257.6692069
24	4.02E+03	244.7774772
26	4.41E+03	233.6453412
28	4.80E+03	223.9057996
30	5.19E+03	215.2907883
32	5.59E+03	207.5993335
34	5.98E+03	200.6773998
36	6.37E+03	194.4046749
38	6.76E+03	188.6856348
40	7.15E+03	183.4433415
42	7.55E+03	178.6150379
44	7.94E+03	174.1489552
46	8.33E+03	170.0019566
48	8.72E+03	166.137771
50	9.11E+03	162.5256488

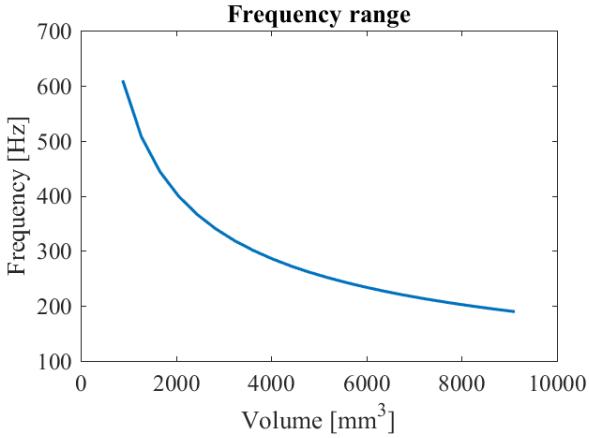

Figure 14: Different cavity volumes and their corresponding frequencies

For the given design frequency range and the precision limitations of the fabrication process, the effective volume of the cavity is varied as a function of the length of the cavity. In the passive design, these lengths are randomly distributed by having a randomizer function in Matlab, over the unit cell array to cover the maximum design frequency range as shown in Figure 16. In the figure, the ridges near the neck of the metamaterial are designed to enable the walls of the metamaterial to slide into a frame. The intended design with the use of the structural frame can be seen in Figure 16. This however is not implemented in the final product, as the mating conformity of the printed products was not effective as a firm support. Furthermore, to test the effect of infill density on the performance, the passive metamaterial is fabricated initially using a gradual infill increase from the neck to the cavity base. The performance of this model is compared with a metamaterial with similar design but with 100% infill.

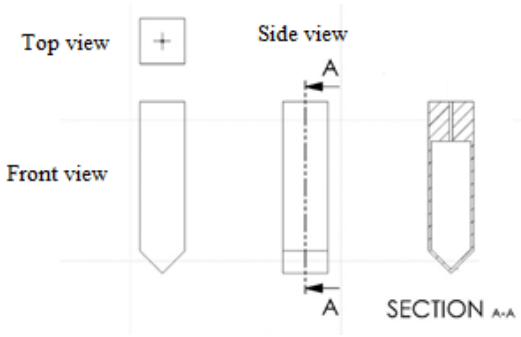

Figure 15: The unit cell structure of the passive metamaterial showing the front, top and section views

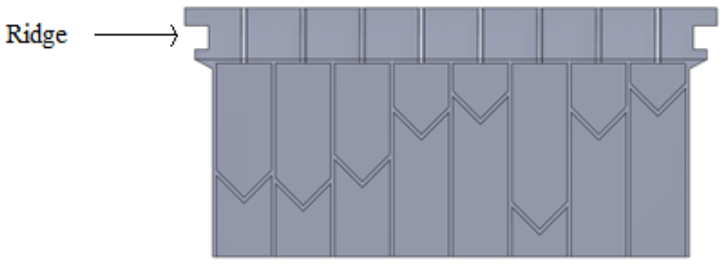

Figure 16: Cross-sectional view of the lattice structure of one wall of the metamaterial showing random cavity depths. In addition, the ridge for sliding the metamaterial wall into the frame is marked

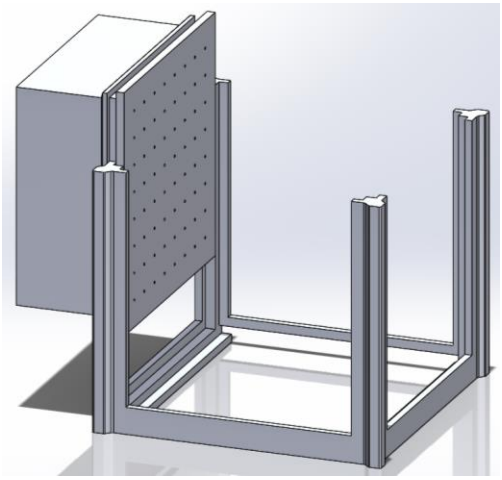

Figure 17: Structural frame design to hold the metamaterial walls

3.1.2 Comparative models

In order to establish a baseline performance comparison for the metamaterial, the system is first tested by using a solid wall of equivalent mass as shown in Figure 18. For this, the mass of the passive metamaterial wall is measured to be 430 g, which is used for the design of the solid wall of same mass. This is hypothesized to provide a reference model to establish a comparison of the performance of a metamaterial against that of non-metamaterial structures.

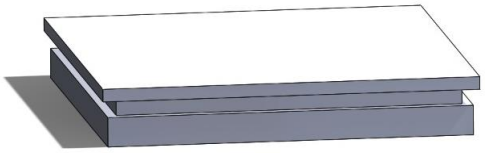

Figure 18: Structure of the solid wall of equivalent mass for comparison

Following the solid model of equivalent mass, another comparison model of a vibro-acoustic metamaterial made by Claeys et al [30] at KU Leuven university is fabricated (Figure 19). This model has been experimentally tested for different arrangements of the resonator unit cells and has been proven to provide significant damping for noise frequencies up to 1000 Hz. Hence, it is expected to provide a proven comparison for the passive metamaterial.

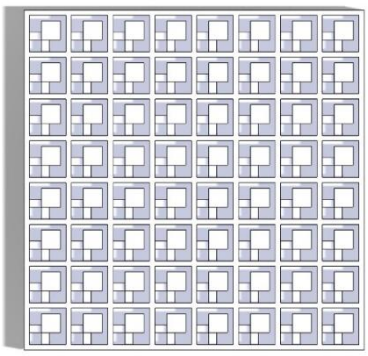

(a)

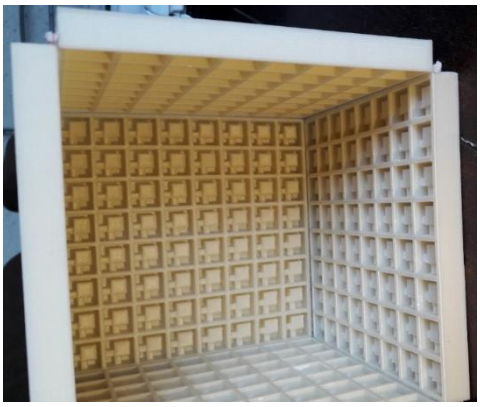

(b)

Figure 19: (a) Schematic top view of a resonator wall of the reference acoustic metamaterial (b) assembled metamaterial with 5 walls [30]

3.1.3 Pneumatically actuated active metamaterial

The passive metamaterial as seen in section 3.1.2 targets a range of broadband frequencies of operation. Although this is indeed useful in attenuating noise levels in the range, targeting isolated frequencies across the range is also important. In a passive design, each individual frequency or each sub-range of frequencies that lie within the targeted range of frequencies requires the fabrication of different models that targets the required particular or sub-range of frequencies. Since this poses a lot of time and material constraints, an active model is proposed, wherein, the volume change of the resonators can be actuated and modified according to the frequency requirements. Thus, a single active model can itself cater to a range or a set of isolated target frequencies, which gives an immense advantage over the passive model. In this design, to vary the volume of each resonator of the metamaterial, the depth of the resonator cavities are varied. As mentioned earlier, the range of depths of the resonator cavities is selected to be from 8 mm to 42 mm. All other dimensions of the active metamaterial are taken from the passive design.

The first method of actuation is through a pneumatic system. A metamaterial wall with the pneumatic actuation method is shown in Figure 20. The outlet of the pneumatic system Figure 21 is connected to an inflatable balloon inside the unit cell. The balloon is attached to the 'V' shaped base of the resonator cavity. As the pressure in the balloon changes, the base of the cavity moves up and down correspondingly, as a result of inflation and deflation of the balloon. The maximum depth of the cavity

is achieved at the deflated phase of the balloon. The only drawback of this mechanism is that accurate depths of the cavities could not be achieved since the commercially available balloons yielded different depths when inflated.

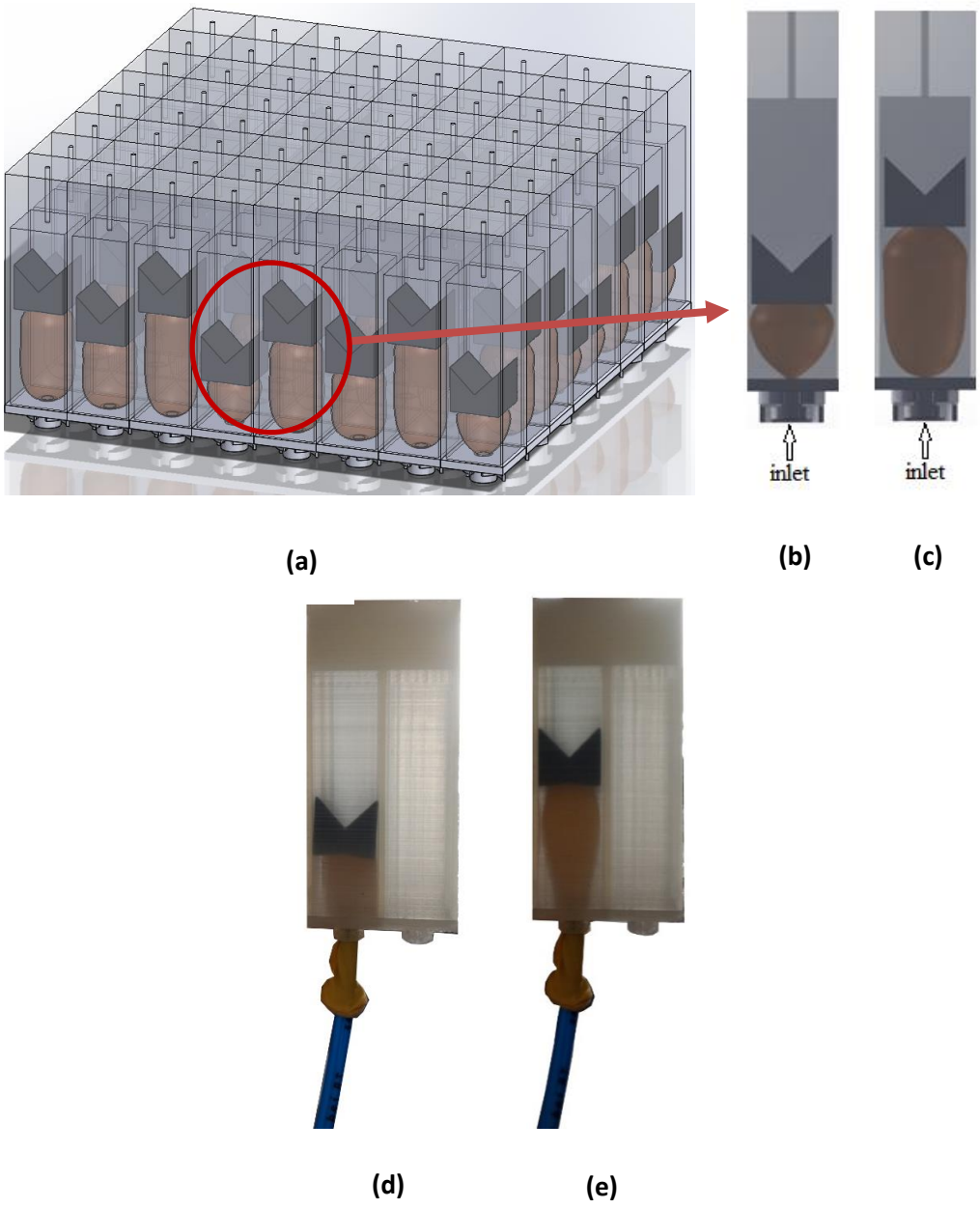

Figure 20: (a) The metamaterial wall containing the balloons; Schematic actuation of the cavity depths with balloons in the (b) deflated (c) inflated state ; Fabricated unit cells with balloons showing the pneumatic mechanism in the (d) deflated (e) inflated state

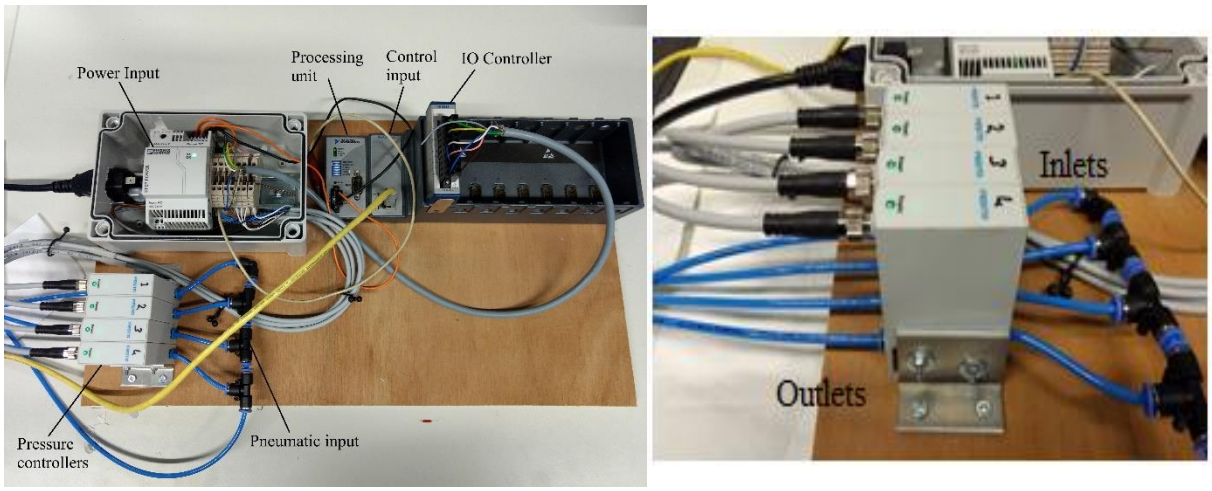

Figure 21: The pneumatic system used for the active metamaterial with the pressure inlets and outlets

3.1.4 Electric actuated active metamaterial

The second actuation method is based on linear control of the depths of the cavities by using a linear motor. The actuation of different cavity depths is controlled by means of a potentiometer connected to the control board of the motor. Each linear motor controls one wall of the metamaterial. Hence, a lattice wall design accommodating 64 cavity bases connected to a common base is made. The linear motor is attached to this base to lift up the wall according to depth requirements. The base of the wall with the 64 cavity bases is designed such that it slides into the cavities of the wall according to the motion of the linear motor thus increasing and decreasing cavity volumes correspondingly. The structure of the designed wall base for the linear actuation is shown in Figure 22. In comparison with the pneumatic case, this mode of actuation has both advantages and drawbacks. In the pneumatic activation, much lower number of actuators are required to create non-uniform distribution of cavity depths whereas the actuation by the linear motor provides a better accuracy of volume change. Furthermore, the pneumatic model, if improved with a good quality of inflatory balloons, can yield different depths of the resonator cavities simultaneously but the linear motor actuation mechanism can have only constant cavity depths at a given point in time. Hence, any increase or decrease in the cavity depths will result in all the cavities of a wall that is controlled by a single motor having a constant depth thus targeting a particular frequency. In this research, due to a limitation in the number of linear motor, constant cavity depths are considered.

To achieve a particular frequency range, the depths can be adjusted in all or a combination of different depths in different walls. One such example is performed during testing the metamaterial performance. Two walls were kept at one depth and the other three walls were kept at a different depth. The results clearly showed two dips in two frequencies corresponding to the two set depths in the metamaterial walls. This type of performance in the metamaterial for a combination of resonator depths is shown in section 4.1.2.

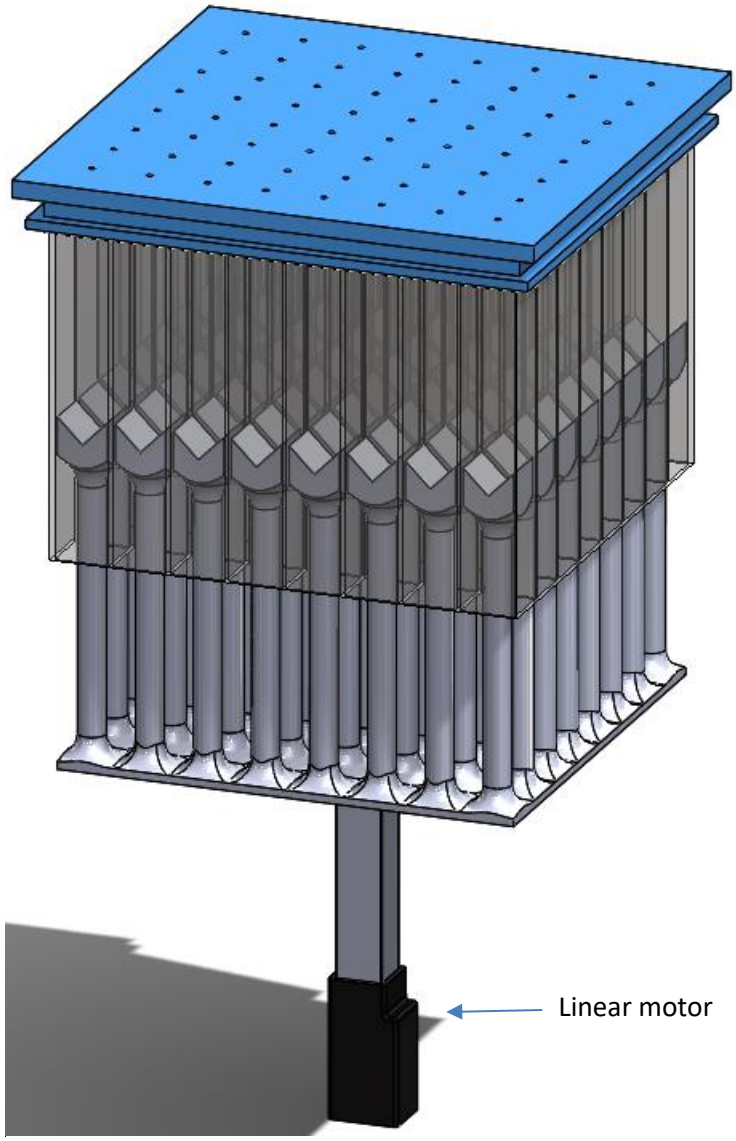

Figure 22: Schematic of the active model containing the cavity bases sliding into the wall cavities by the action of the linear motor attached to the base

3.2 Fabrication

As mentioned earlier, the method of fabrication chosen for the models is additive manufacturing (AM), commonly known as 3D printing. Additive manufacturing has been a tool that is widely used as a manufacturing process and has been proven greatly useful for the fabrication of intricate details in various structures. This section brings to light some of the highlights of AM that was the main process of fabrication in this project.

Additive manufacturing (AM) is a processing method that is being used for the ease of fabrication of structures with various classes of materials including metals, polymers, ceramics, etc. The process involves layering of a suitable material to form a specified three-dimensional structure where the user through a computer software provides the geometrical specifications. This is very useful for various applications because of the completion of the process by simple layering without the use of molds or heavy machines. Since in the current world, polymers have a wide variety of applications, it is therefore important to improve the manufacturing processes thereby making it simple, less time consuming and

less expensive. By Additive manufacturing, it is possible to manufacture complex parts with intricate details in a relatively lesser amount of time. In general, there are three main methods of AM: stereo lithography (SLA), selective laser sintering (SLS) [48, 49] and fusion deposition modelling (FDM) [50-52]. Since the fabrication resources are restricted to Fused deposition modelling for this project, some basic concepts of FDM are briefly explained here. Fused Deposition modelling uses a layer-by-layer printing technique. When the filament is provided to the machine, the material is first liquefied by heating to its melting temperature. This liquefaction of the material is required to ease the extrusion process that follows. Meanwhile, the build plate is also heated to aid the adhesion of the material to the build plate to prevent delamination or warping of the model. Based on the input design that is provided using a software, the material is printed layer by layer on the heated build plate. The material layers are then left to cool down to room temperature for proper interlayer bonding. A schematic of the FDM process is shown in Figure 23.

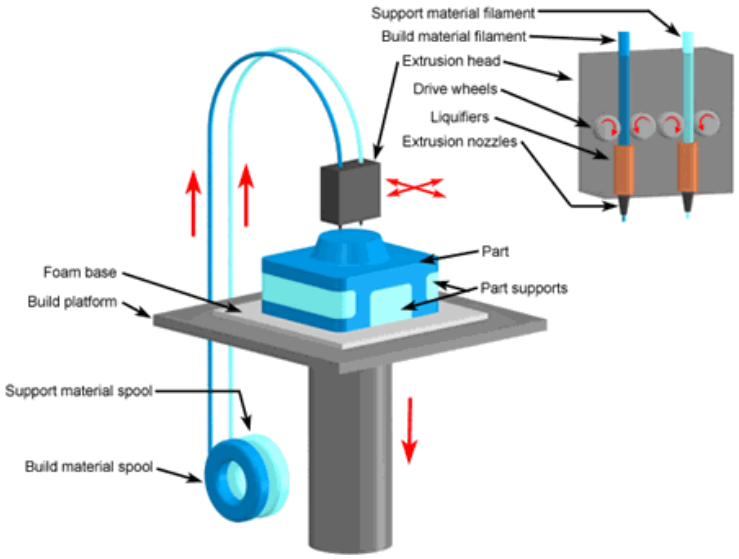

Figure 23: Schematic of the FDM process [53]

The FDM apparatus used for this project is the Ultimaker 2+ and Ultimaker 3 3D printers (Figure 24). The Ultimaker 3 has a double extruder system that enables printing two materials at the same time while the Ultimaker 2+ has a single extruder. In addition, The 2+ model has a layer height of 0.15 mm and the Ultimaker 3 has a layer height of 0.2 mm. The layer height is a parameter that affects the fineness of the model and the speed of printing.

(a) **(b)**

Figure 24: Image of the 3D printers used (a) Ultimaker 3 (b) Ultimaker 2+

Problems encountered during fabrication include

- Build plate area of the printer was restricted to 210×210 mm^2 which led to a restriction in the maximum metamaterial dimensions and the number of unit cells
- A maximum overhang angle of 50 degrees was allowed for the design of the models after which support structures were formed. This constraint had to be taken into account while designing the resonator cavities. After considerations, the 'V'-shaped structure was designed in order to avoid the formation of support structures while printing
- The printer nozzle needed to be cleaned frequently to avoid nozzle clogging which resulted in the failure of the print
- Wide prints tended to warp due to non-uniform cooling of the print volume and ineffective print bed heating at the print edges of the build plate which affected the build plate adhesion

3.3 Experimental set-up

Post fabrication, for the purpose of taking acoustic measurements, two measurement paradigms were selected: an open system and a closed system. The arrangement was chosen to be cubic in nature for ease of assembly and conformity of both systems. The open system was designed to consist of four metamaterial walls arranged along the perimeter of a square, held together by a frame, while the closed system was designed to the same base structure of the open system with an additional wall closing the top section of the setup.

3.3.1 Open system

The open setup consists of the metamaterial with four walls arranged in a cubical shape (Figure 25). An aluminium tube is placed on either side of the metamaterial to mimic an open tunnel. A speaker is placed at one end of the tube and a microphone is placed on the other end to measure the noise attenuated after interacting with the metamaterial (Figure 25). The measurements of the passive metamaterial wall was also compared with the solid wall structure and the KU Leuven acoustic metamaterial with the same setup.

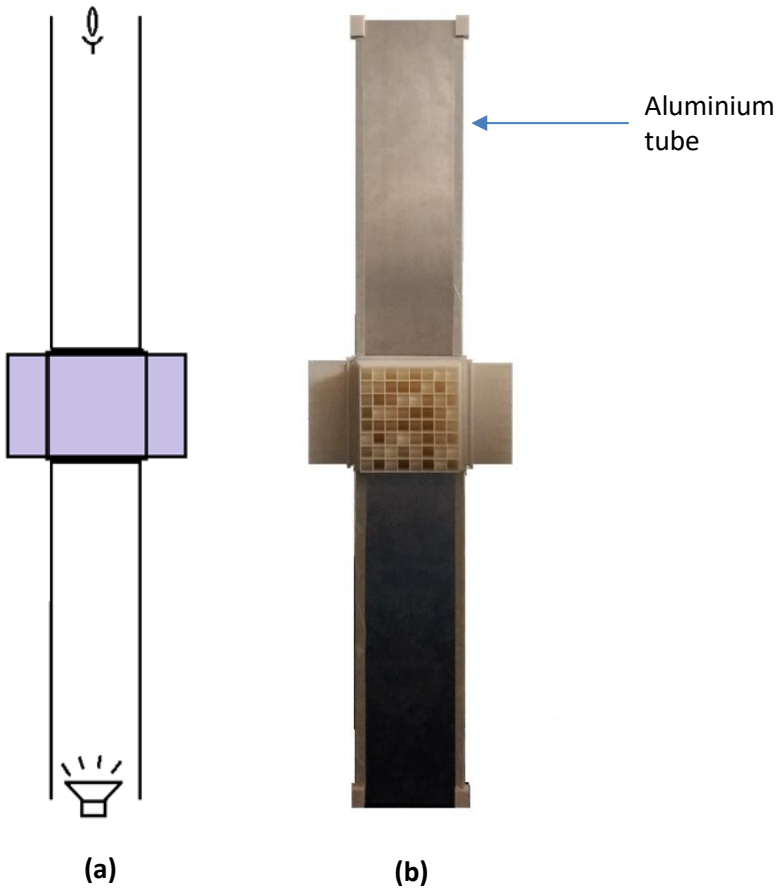

Figure 25: (a) Schematic of the open system with the speaker at the bottom and the mic on the top to record the attenuated noise. The grey region represents the four walls of the metamaterial (b) Experimental setup of the open system with the metamaterial walls and the aluminium tube

3.3.2 Closed system

The closed system is aimed at recreating the environment of a soundproof room. This is constructed with five walls of the metamaterial structure in a cubical shape with one end for the speaker such that the five metamaterial walls cover the speaker from all sides (Figure 26). Since the objective of the setup is to seal the noise from the speaker without exiting the space inside the metamaterial, the sound recording device is kept outside the system at a certain distance of 15 cm from the metamaterial walls.

This distance is maintained constant for all the measurements to ensure that there is no change in the amplitude of the noise levels measured due to changing the distance of the mic.

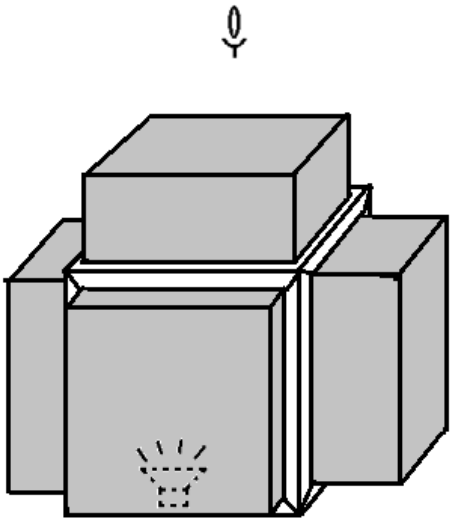

(a)

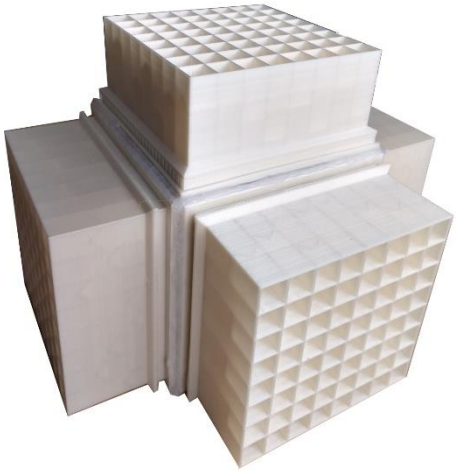

(b)

Figure 26: (a) Schematic of the closed system with the speaker inside the system and the mic outside to record the attenuated noise (b) Experimental setup of the closed system with the mic kept inside

3.3.3 Pneumatic actuation

As explained in the previous section, the active metamaterial is actuated by two types of mechanisms. The first one is the pneumatic actuation wherein the pneumatic outlets from the system are connected to inflatable balloons that change the depth of the cavities according to the input pressures. Since the number of outlets from the pneumatic system is restricted to four, a splitter is made for each outlet such that each pressure outlet is distributed to more outlets (Figure 27a). The design of the splitter is also shown in Figure 27b and 26c. The closed setup needs the use of five metamaterial walls with 64 resonators each and hence 80 outlets are drawn from one pressure outlet.

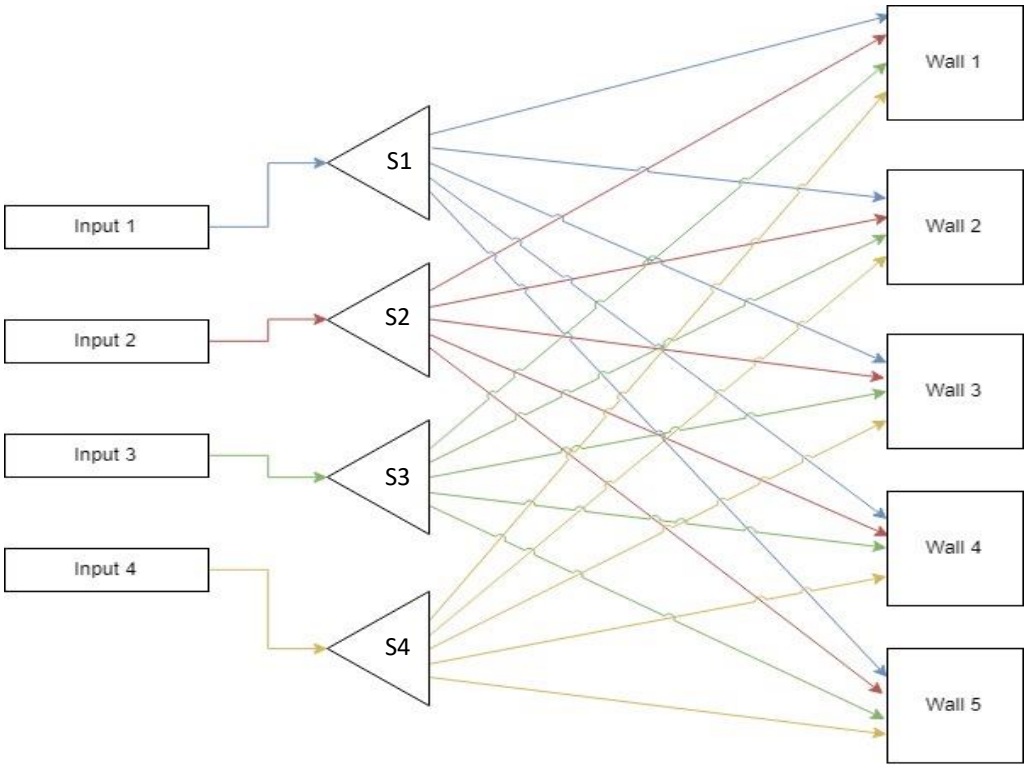

(a)

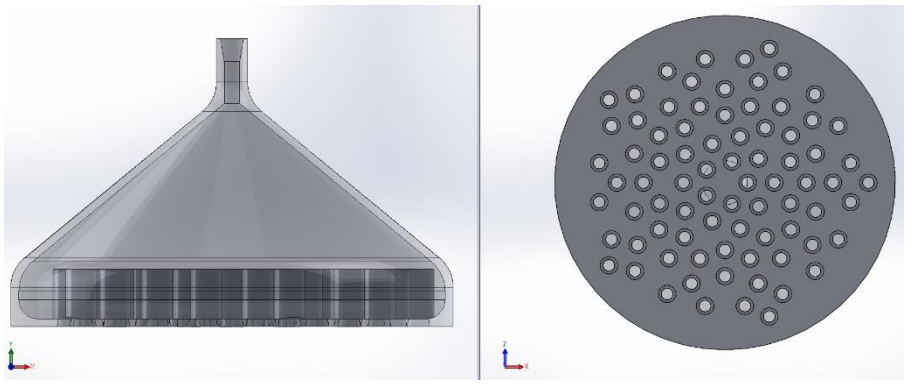

(b) **(c)**

Figure 27: (a) Schematic of the pneumatic actuation system showing the inputs from the system, and the distributed outputs from the splitters (S1, S2, S3 and S4 represent the splitters and the colors represent the outputs from each splitter) (b) Front view of the splitter (c) Bottom view of the splitter

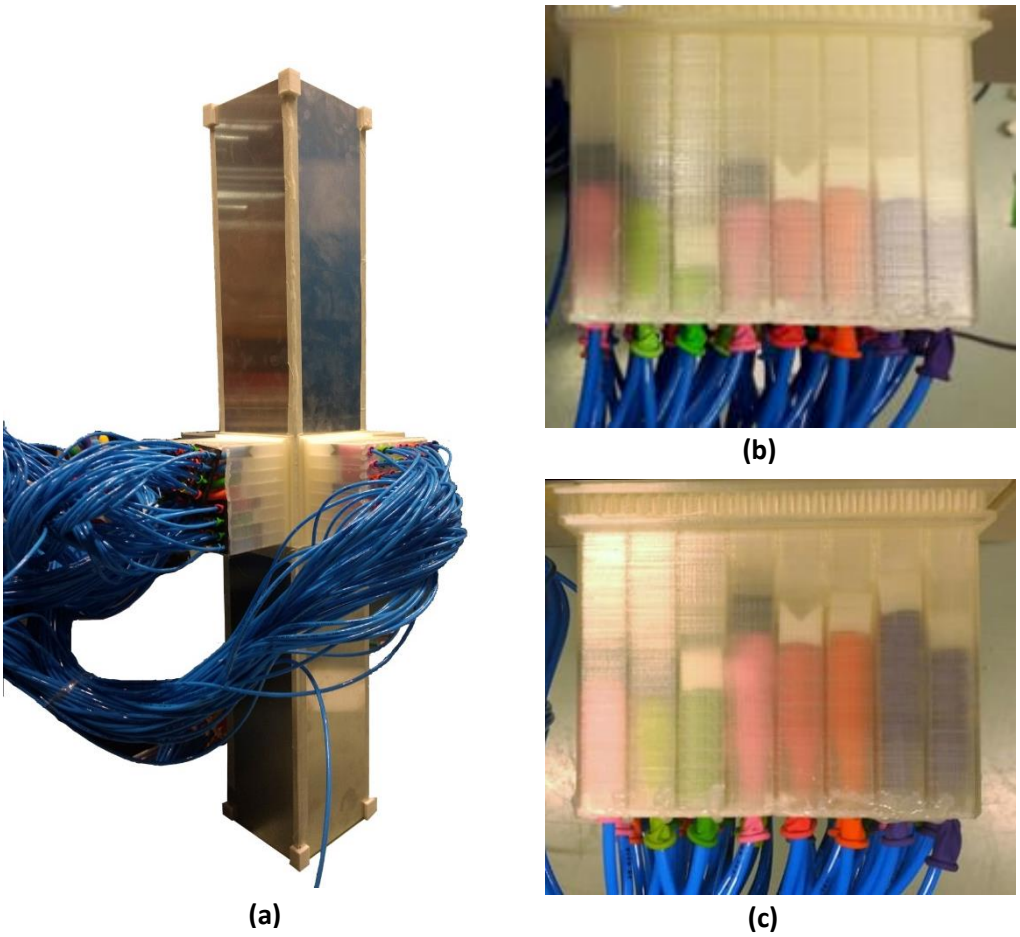

Figure 28: (a) Experimental setup of the pneumatic actuation showing the pressure outlets from the pneumatic system connected to the inflatable balloons inside the resonator cavities (b) Cavity depths at P=0.05 bar (c) Cavity depths at P=0.15 bar

The pressure outlet is connected by means of pressure tubes to the balloons fixed inside the resonator. The balloons are inserted through the backplate, which seals the resonator cavity after being glued to the cavity bases. Figure 28 shows the whole setup in the open system with the four pressure outlets connected to the resonators by means of the splitter. Furthermore, the different cavity depths for the two different pressures are also shown. The metamaterial is tested at two pressures, the former corresponding to the lowest pressure to achieve the highest possible cavity depths, and the latter corresponding to the maximum pressure before which the cavity depth becomes zero. Since the open system needs only four walls, the remaining 64 outlets are sealed.

3.3.4 Electric linear actuation setup

In order to have a better control over the precision of the depth change, a second method of actuation is chosen. A micro linear actuator of model L12-5-210-12-P from Actuonix motion devices Inc., Canada, controlled by a potentiometer input is used. To control the position of the actuator head, a control board (Actuonix L.A.C) is used to act as an interface between the potentiometer and the linear motor (Figure 29). The actuator in its fully extended state is shown in Figure 29b. The actuator has a precision of about 0.5 mm and a maximum range of 50 mm. Since the range of the cavity depths is around 40

mm, the actuator is suited to the purpose. Figure 30 shows the linear motor installed on to a metamaterial wall.

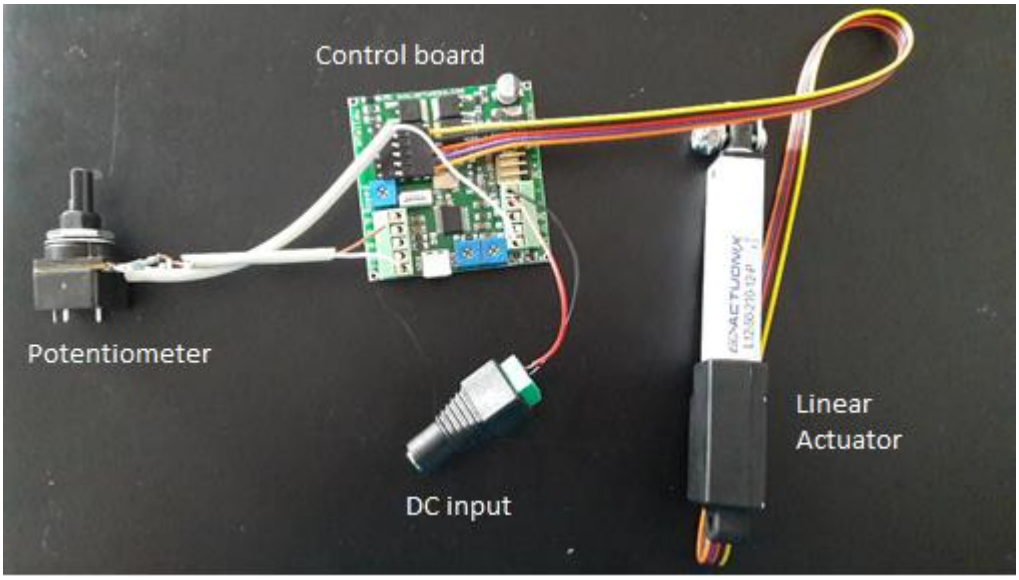

(a)

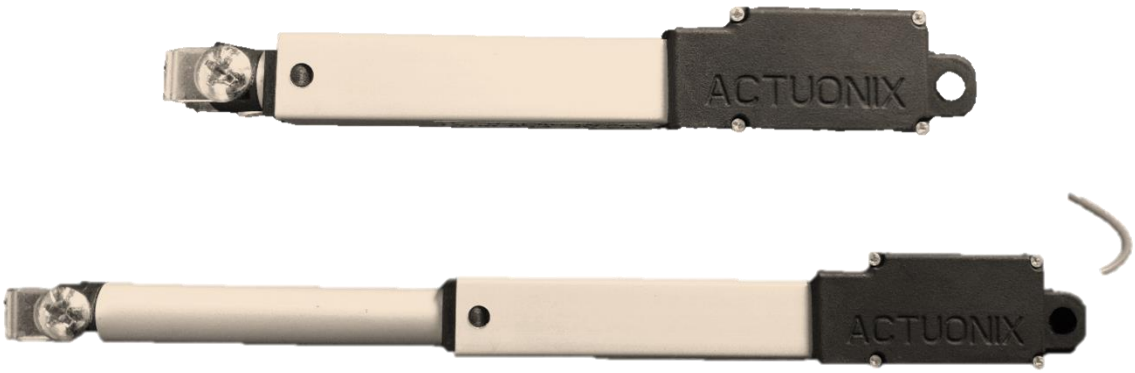

(b)

Figure 29: (a) Control circuit with potentiometer, control board and the linear actuator (b) The linear actuator in its fully contracted and extended states

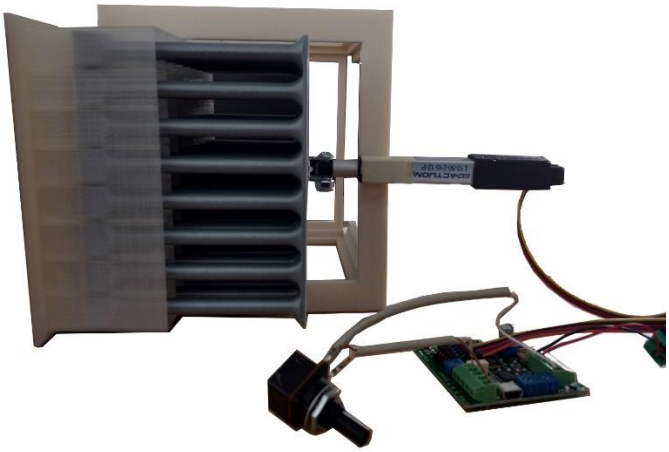

(a)

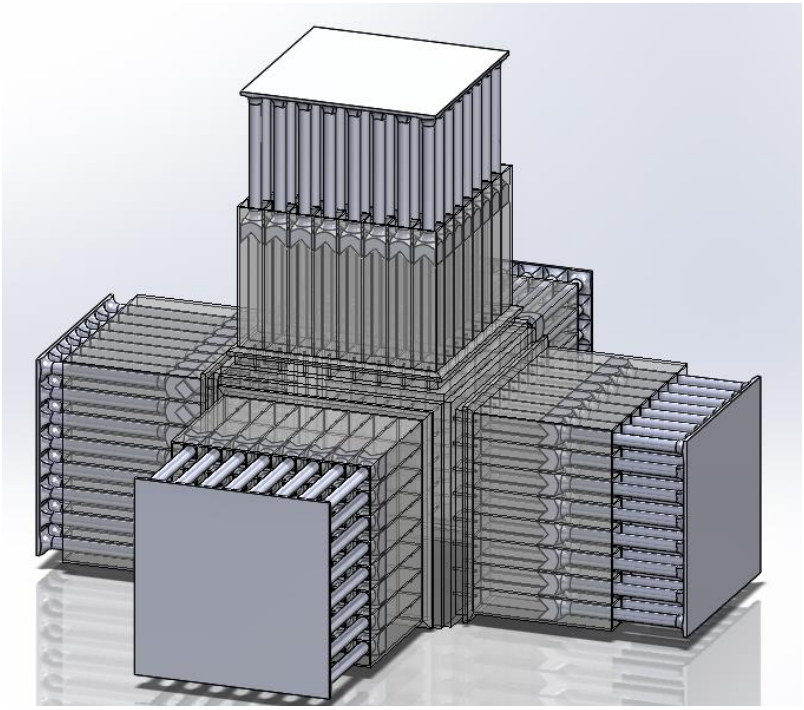

(b)

Figure 30: (a) Metamaterial wall installed with the linear motor circuit (b) Schematic of the five metamaterial walls with five different cavity depths

3.3.5 Noise types and measurement techniques

After arranging the test setup for the open and the closed systems, the noise samples for experimentation are chosen. The noise samples were all acquired from a tone generator application. The noise attenuation levels are measured with a microphone for different frequencies and are plotted

to determine the performance of the metamaterials. Here, a Sennheiser e908B cardioid condenser microphone that has a frequency response of 40 – 20000 Hz is used as the recording instrument (Figure 31).

Figure 31: Sennheiser e908B cardioid condenser microphone used for testing

The different noise samples chosen for testing are as follows:

- White noise
  White noise is a form of sound produced from a continuum of all the frequencies in the hearing range that are distributed in a random manner equally over the range. This sample is chosen as it has uniformly distributed loudness for all frequencies (Figure 32)
- Pink noise
  Pink noise has essentially the same effect and construction as the white noise, except that it concentrates more on the lower end of the frequency spectrum (Figure 32) and hence is more soothing to listen to as compared to white noise.
- Brown noise
  Brown noise also has the same constituent frequency range as white noise but is more composed of lower frequencies than pink noise (Figure 32). Pink and brown noise samples are chosen to provide a variety of samples with continuous frequencies
- Assorted isolated frequencies in the range of 100 Hz to 5000 Hz to evaluate the range of frequencies of operation of the metamaterials
- A frequency sweep from 10000 Hz to 20 Hz to provide a wide range of separated frequency noises while measuring loudness in real time

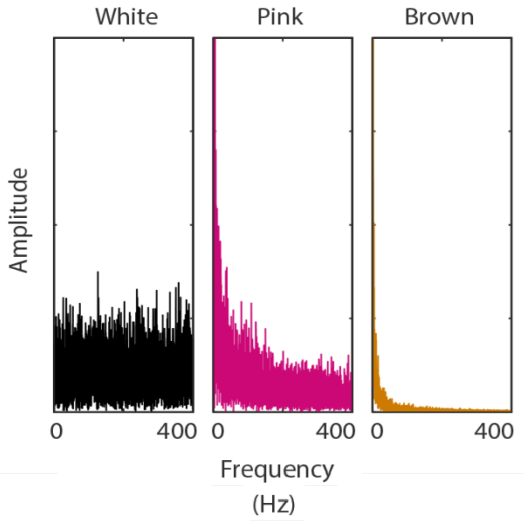

Figure 32: Frequency spectrums of white, pink and brown noise showing difference in amplitude for the respective frequency domains [54]

In the results shown for the performance of the active and the passive metamaterials, the sound pressure levels (SPL) are obtained by taking a fast Fourier transform of the recorded sound clips, thus changing the output from a time domain plot to a frequency domain plot. These plots are normalized with respect to a reference ambient pressure plot.

4

Results and discussions

4.1 Passive metamaterial

The passive metamaterial is designed to attenuate frequencies between 150 Hz and 450 Hz, as described in section 4.1.1. The obtained frequency response and the hypothesized implications are discussed in this section.

4.1.1 Open system

The performance of the open system for the designed range of frequencies shows a substantial attenuation of frequencies up to 400Hz while investigated with isolated frequency inputs (Figure 33). The effect of the resonators decays towards the higher frequency range, as predicted from the design range of attenuation. In some plots, there can be seen, a sinusoidal wave like variation (Figure 33p) that can be seen as a result of the wavering nature of the frequency output of the speaker unit. This can be confirmed from the blue dotted lines representing the baseline plot measured with only the speaker and no metamaterial on top also showing the same type of variation. From the plots of white and brown noise, it can be said that the metamaterial provides a reasonable attenuation (10–20 dB) for frequencies up to 600Hz. The metamaterial also attenuates sound up to 1000 Hz. This is likely due to fabrication inaccuracies, especially because of the changing dimensions of the neck diameter that might have altered the operational frequency range though the design is intended for lower frequencies up to 500 Hz. Finally, from these graphs, a maximum attenuation of around 20 dB i.e., the difference in the amplitudes of the solid wall case (blue dotted line) and the passive metamaterial case (yellow line), at a frequency of approximately 150 Hz can be seen from the graphs in Figure 33b.

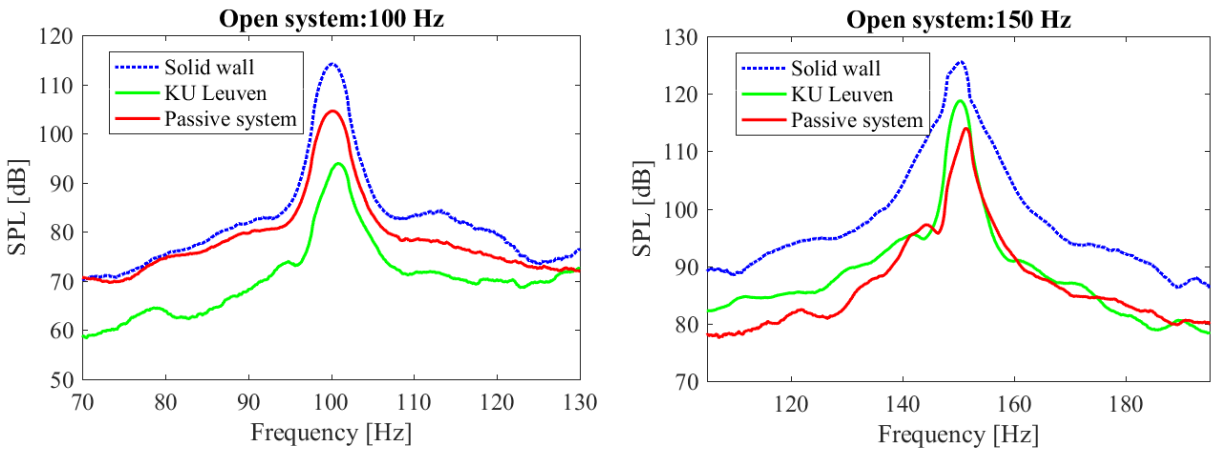

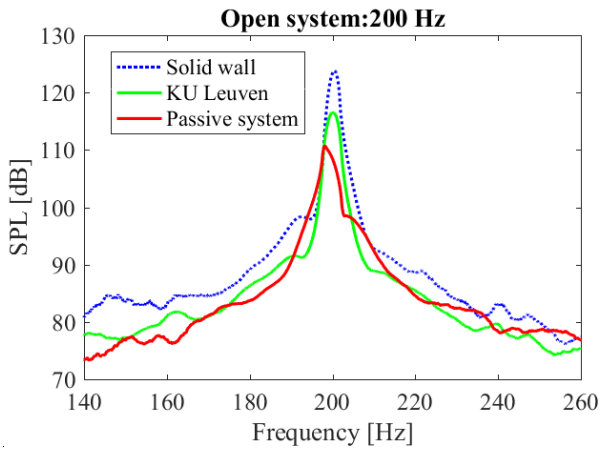
Open system:200 Hz
Solid wall
KU Leuven
Passive system
SPL [dB]
Frequency [Hz]

(c)

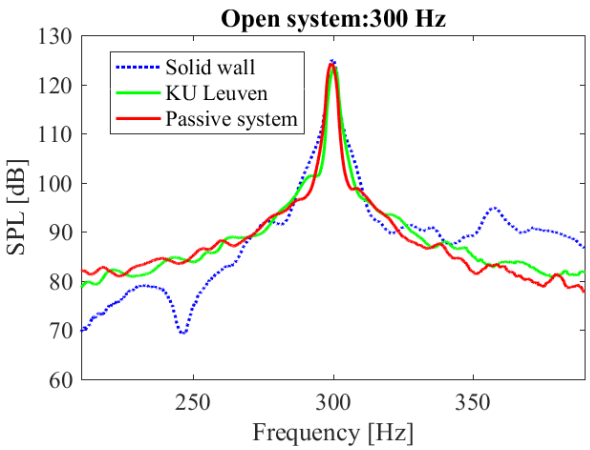
Open system:300 Hz
Solid wall
KU Leuven
Passive system
SPL [dB]
Frequency [Hz]

(d)

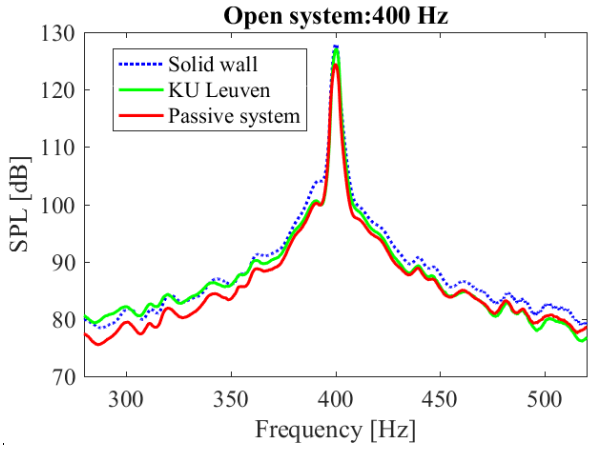
Open system:400 Hz
Solid wall
KU Leuven
Passive system
SPL [dB]
Frequency [Hz]

(e)

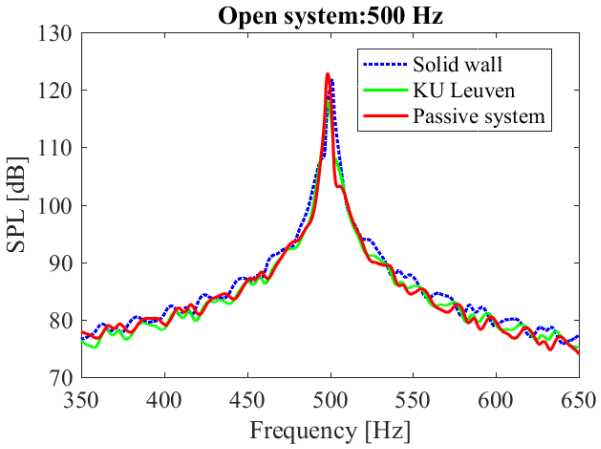
Open system:500 Hz
Solid wall
KU Leuven
Passive system
SPL [dB]
Frequency [Hz]

(f)

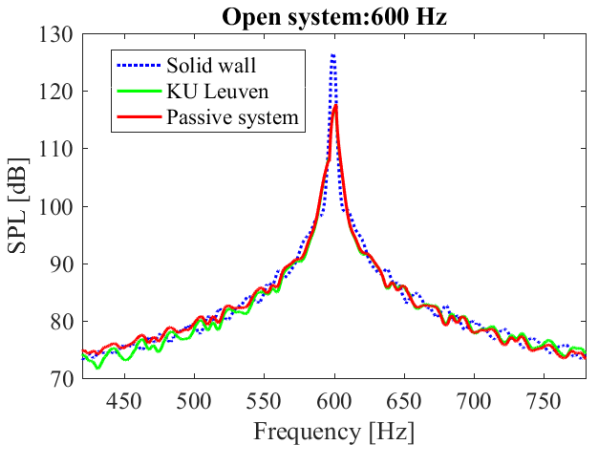
Open system:600 Hz
Solid wall
KU Leuven
Passive system
SPL [dB]
Frequency [Hz]

(g)

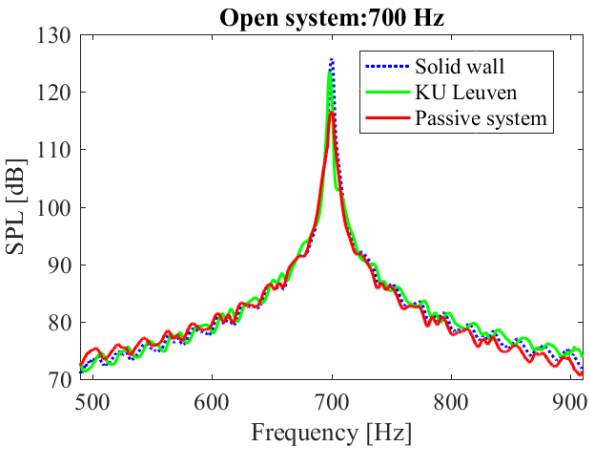
Open system:700 Hz
Solid wall
KU Leuven
Passive system
SPL [dB]
Frequency [Hz]

(h)

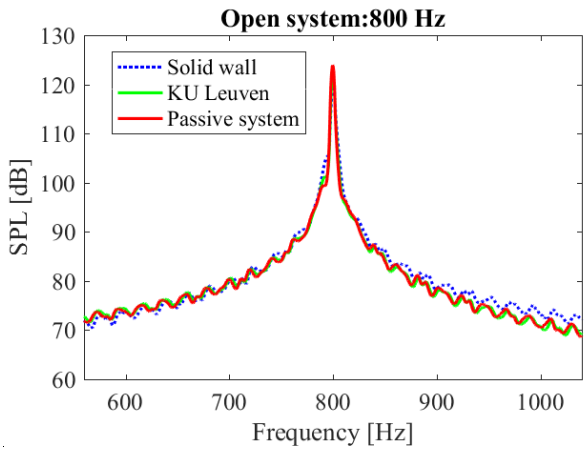
Open system:800 Hz
Solid wall
KU Leuven
Passive system
SPL [dB]
Frequency [Hz]

(i)

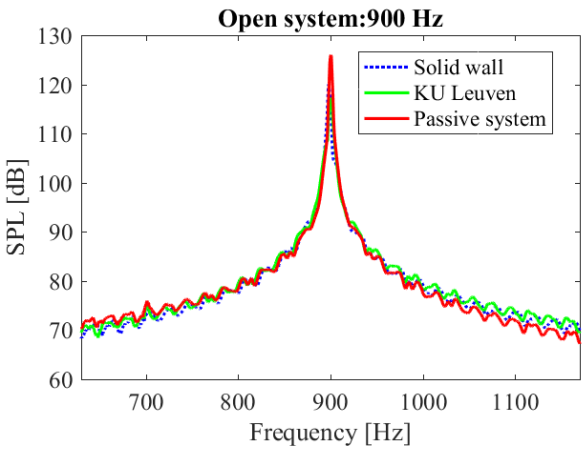
Open system:900 Hz
Solid wall
KU Leuven
Passive system
SPL [dB]
Frequency [Hz]

(j)

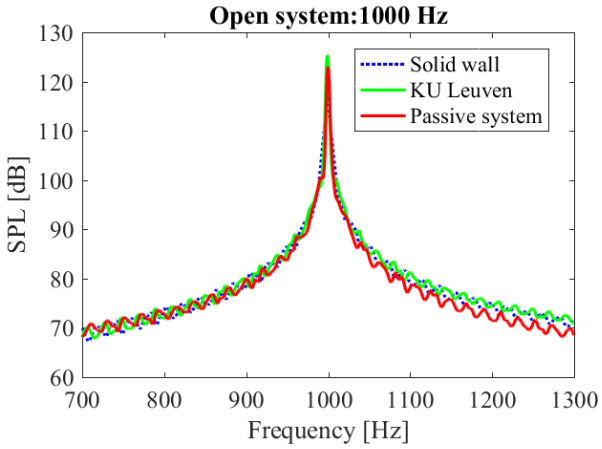
Open system:1000 Hz
Solid wall
KU Leuven
Passive system
SPL [dB]
Frequency [Hz]

(k)

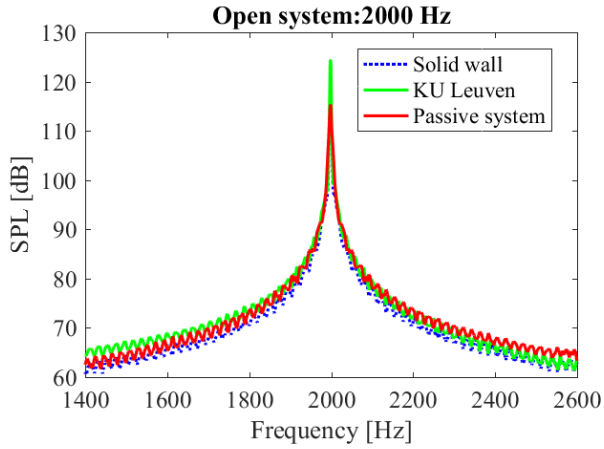
Open system:2000 Hz
Solid wall
KU Leuven
Passive system
SPL [dB]
Frequency [Hz]

(l)

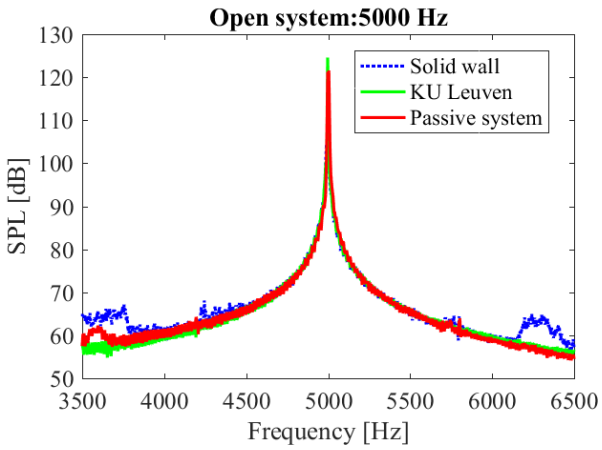
Open system:5000 Hz
Solid wall
KU Leuven
Passive system
SPL [dB]
Frequency [Hz]

(m)

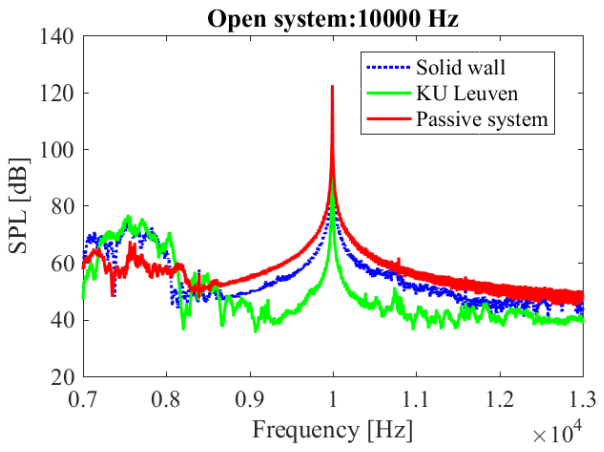
Open system:10000 Hz
Solid wall
KU Leuven
Passive system
SPL [dB]
Frequency [Hz]
×10^4

(n)

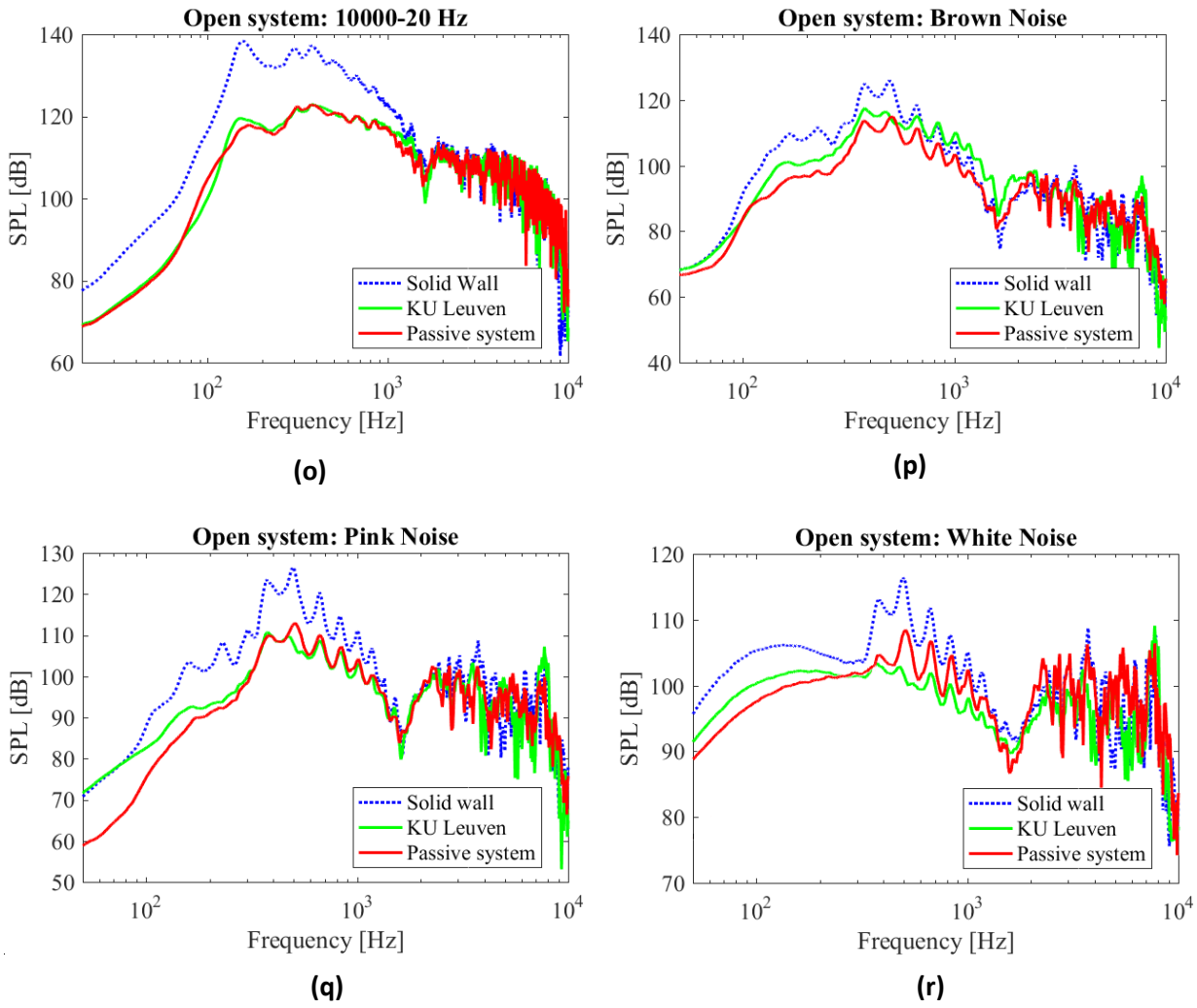

Figure 33: Measured noise amplitude levels in the open system setup for different noise samples including pink and brown noise, isolated frequencies and frequency sweep from 10000 - 20 Hz showing the amount of attenuation achieved for each case

4.1.2 Closed system

As compared to the open system, the closed system shows a significantly higher attenuation over a larger range of frequencies. On comparison with a solid PLA wall system of comparable mass, this is quickly attributed to the attenuation caused by a solid enclosure. The attenuation beyond the solid wall response is hence taken as the effective result of the presence of resonators. Beyond the solid wall effect, the resonators provide for up to 25dB of attenuation between frequencies of 100Hz and 500Hz, after which the effect of the resonators quickly decays as shown in the plots in Figure 34p.

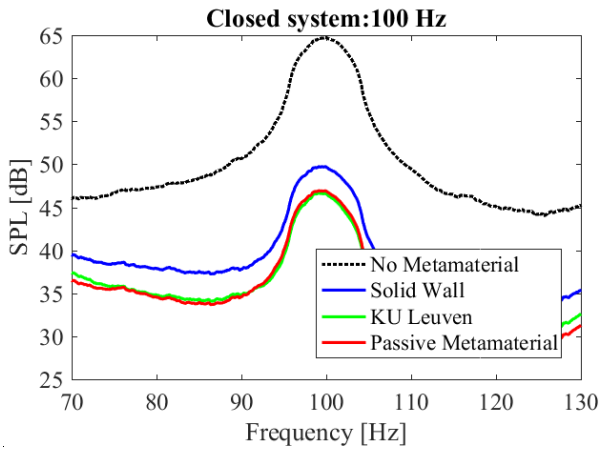
Closed system:100 Hz
SPL [dB]
Frequency [Hz]
No Metamaterial
Solid Wall
KU Leuven
Passive Metamaterial

(a)

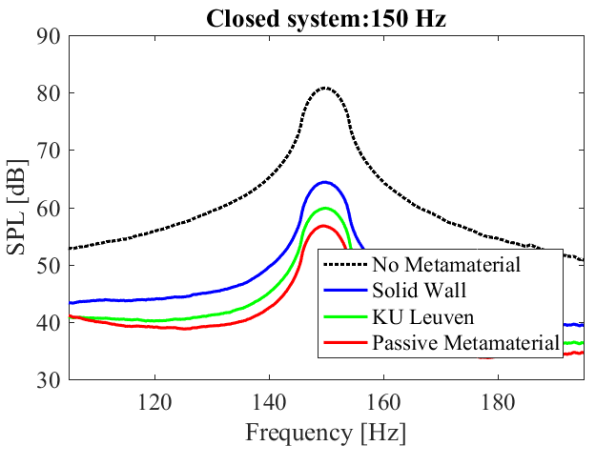
Closed system:150 Hz
SPL [dB]
Frequency [Hz]
No Metamaterial
Solid Wall
KU Leuven
Passive Metamaterial

(b)

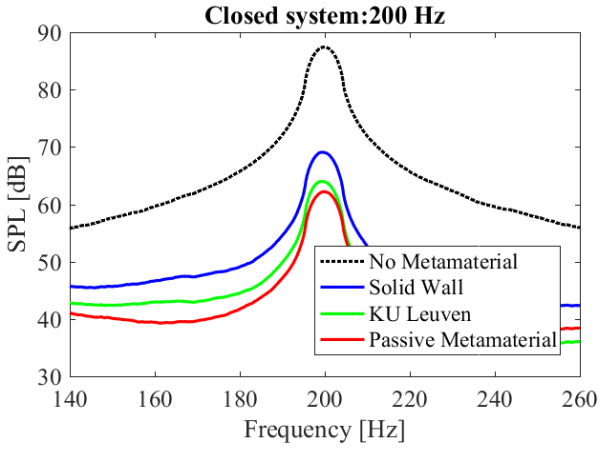
Closed system:200 Hz
SPL [dB]
Frequency [Hz]
No Metamaterial
Solid Wall
KU Leuven
Passive Metamaterial

(c)

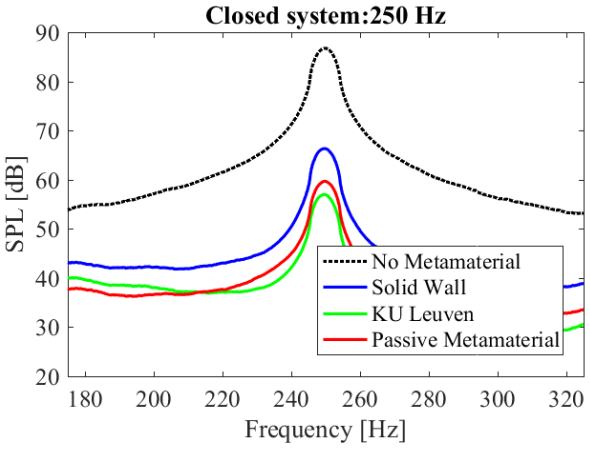
Closed system:250 Hz
SPL [dB]
Frequency [Hz]
No Metamaterial
Solid Wall
KU Leuven
Passive Metamaterial

(d)

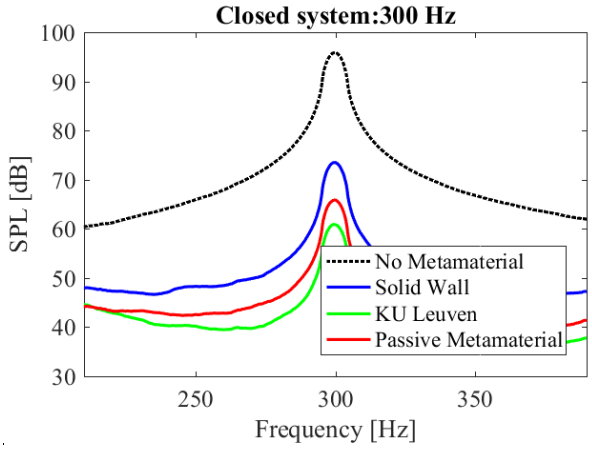
Closed system:300 Hz
SPL [dB]
Frequency [Hz]
No Metamaterial
Solid Wall
KU Leuven
Passive Metamaterial

(e)

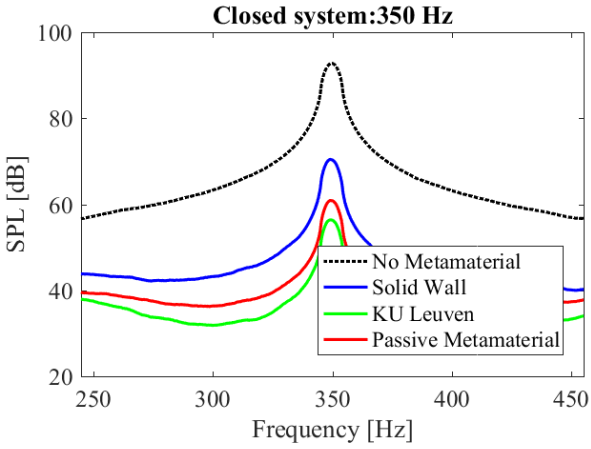
Closed system:350 Hz
SPL [dB]
Frequency [Hz]
No Metamaterial
Solid Wall
KU Leuven
Passive Metamaterial

(f)

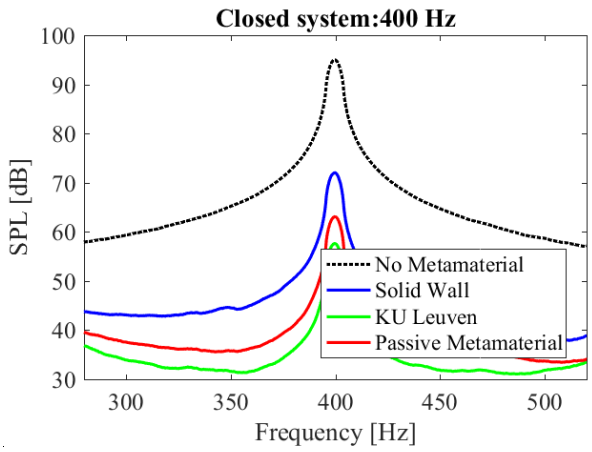
Closed system:400 Hz
SPL [dB]
Frequency [Hz]
No Metamaterial
Solid Wall
KU Leuven
Passive Metamaterial

(g)

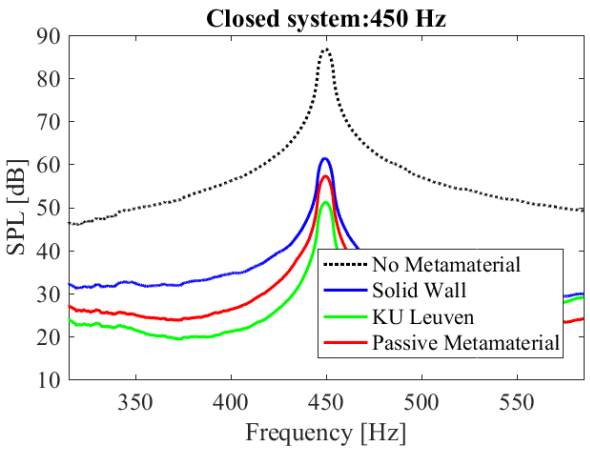
Closed system:450 Hz
SPL [dB]
Frequency [Hz]
No Metamaterial
Solid Wall
KU Leuven
Passive Metamaterial

(h)

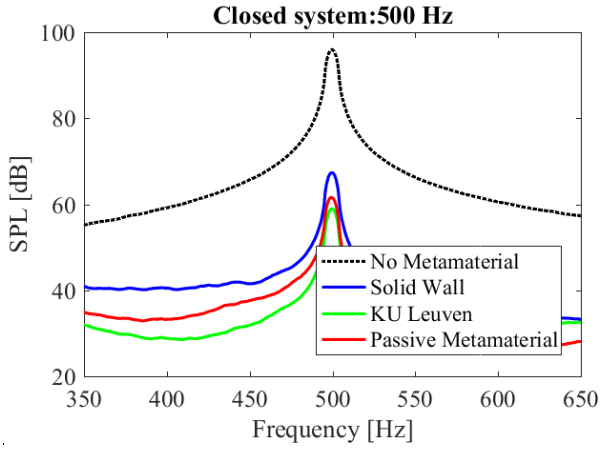
Closed system:500 Hz
SPL [dB]
Frequency [Hz]
No Metamaterial
Solid Wall
KU Leuven
Passive Metamaterial

(i)

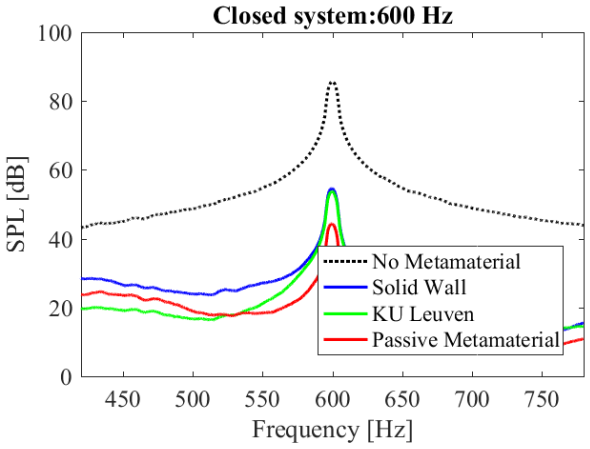
Closed system:600 Hz
SPL [dB]
Frequency [Hz]
No Metamaterial
Solid Wall
KU Leuven
Passive Metamaterial

(j)

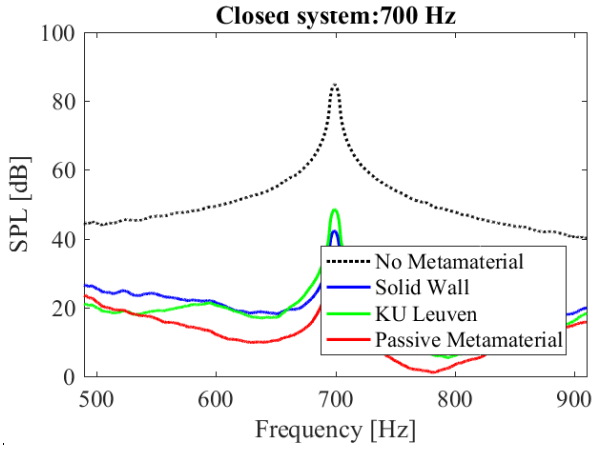
Closed system:700 Hz
SPL [dB]
Frequency [Hz]
No Metamaterial
Solid Wall
KU Leuven
Passive Metamaterial

(k)

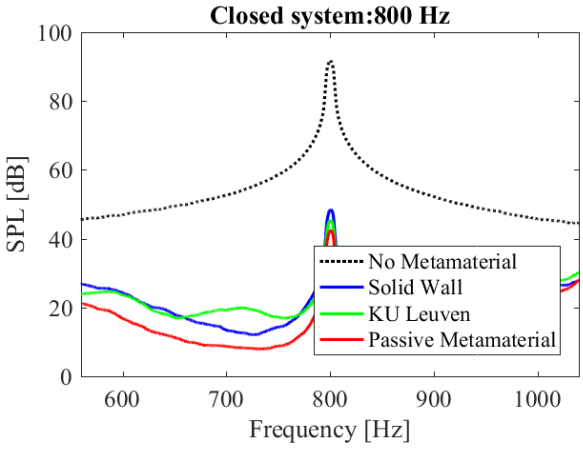
Closed system:800 Hz
SPL [dB]
Frequency [Hz]
No Metamaterial
Solid Wall
KU Leuven
Passive Metamaterial

(l)

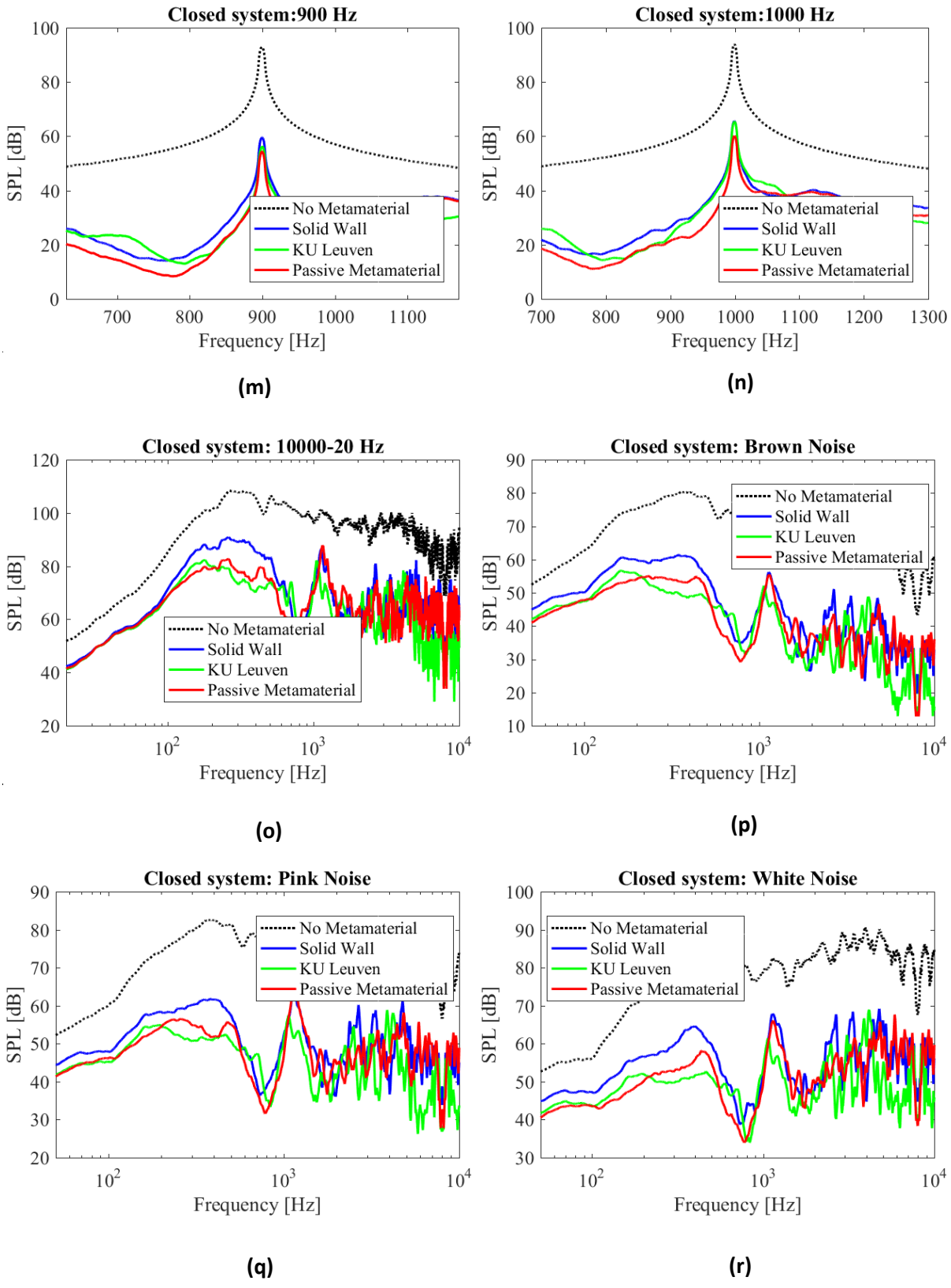

Figure 34: Measured noise amplitude levels in the closed system setup with the speaker inside the 5 walls of the metamaterial for different noise samples including pink and brown noise, isolated frequencies and frequency sweep from 10000 - 20 Hz showing the amount of attenuation achieved for each case

From the results showing the performance of the passive metamaterial in the closed and the open systems, it can be seen that the closed system provides more attenuation than the open system. This

can be seen as the dynamics the noise transmission is very much different in the closed and the open systems. In addition, a comparison between the two systems might be unfair as even the distance from the source to the mic is different which also plays an important role in noise measurements. Figure 35 shows the comparison of the attenuation performance of the models at different frequencies. It is notable that in the closed system plots, a maximum attenuation 50 dB is recorded at around 800 Hz. However, this cannot be considered in it entirety as a contribution of the passive metamaterial as it is seen that the solid wall model also gives a higher attenuation around that frequency. This proves that at frequencies higher than the target frequencies (500 Hz), the attenuation might not be entirely due to the effect of the resonators but simply due to the fact that there is any obstruction around the sound source. Thus in order to identify the effectiveness of the resonators, it would be wise to compare it with the effect of the solid model of the same mass than to the base case. By taking this into consideration, the maximum attenuation of the passive metamaterial compared to the solid model come to about 10 dB at 350 Hz. As for the open system, since the solid wall and the base case is the same, the maximum attenuation observed is 18 dB at a frequency of 150 Hz. This cannot be taken as a performance metric of the closed system against the open system for two reasons. Firstly, the dynamics of the closed system is completely different compared to the open system and secondly, the reference curves for the two systems are completely different. In addition, in comparison with the KU Leuven acoustic metamaterial, the passive model performs better in the closed system from about 250 Hz to 500 Hz. The performance of the KU Leuven model can however not be predicted as the results show a better performance for some frequencies and lower attenuation at others. In the open system measurements, the passive model is found to achieve more attenuation than the KU Leuven model for frequencies below 800 Hz Figure 35a. Furthermore, it is unknown if the performance of the KU Leuven metamaterial scales linearly as a scaled down model of the metamaterial was used as reference.

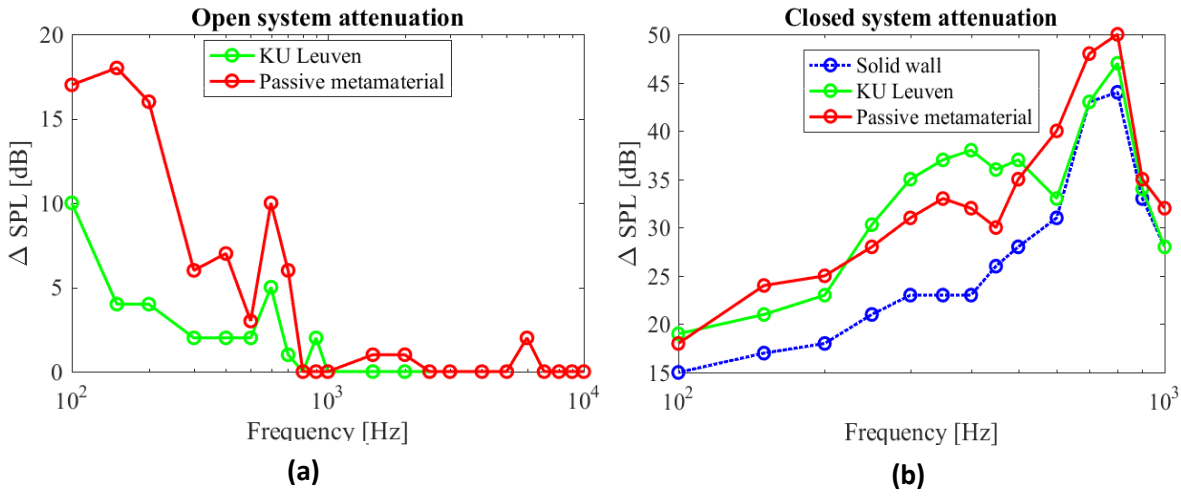

Figure 35: Comparison of attenuation performances of the solid, KU Leuven and the passive models for the (a) open and (b) closed system

4.1.3 Effect of infill density

During the fabrication process, reducing the infill density of the prints lowers the printing duration significantly. However, it is necessary to establish whether the reduced mass density makes the system

less effective. For this reason, two passive metamaterial models with different infill densities were fabricated as explained in section 3.1.1. The measured weights of gradual infill and the 100% infill metamaterial walls are approximately 330 g and 430 g respectively. The plots of white and pink noise samples observed against a 100% infill metamaterial and a graded infill metamaterial are described in Figure 36. It is noticed that the effect of infill density is not significant to the performance of the resonators of the metamaterial in most cases. However, this cannot be conclusively proven as the sample space is small and the infill rather than being uniform is a uniformly varying infill. Although the evidence cannot be considered as conclusive proof of independence, it points towards a potential hypothesis.

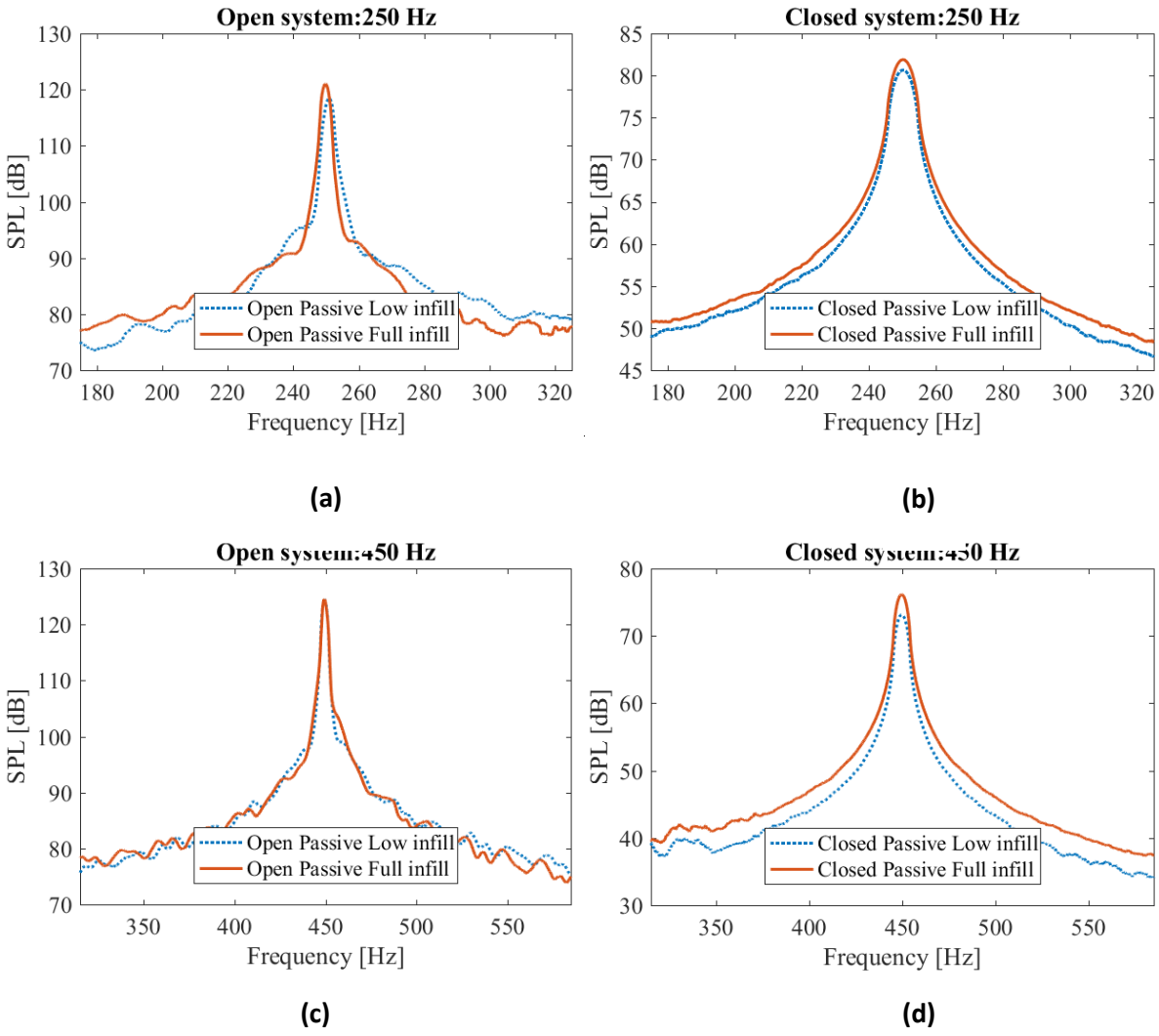

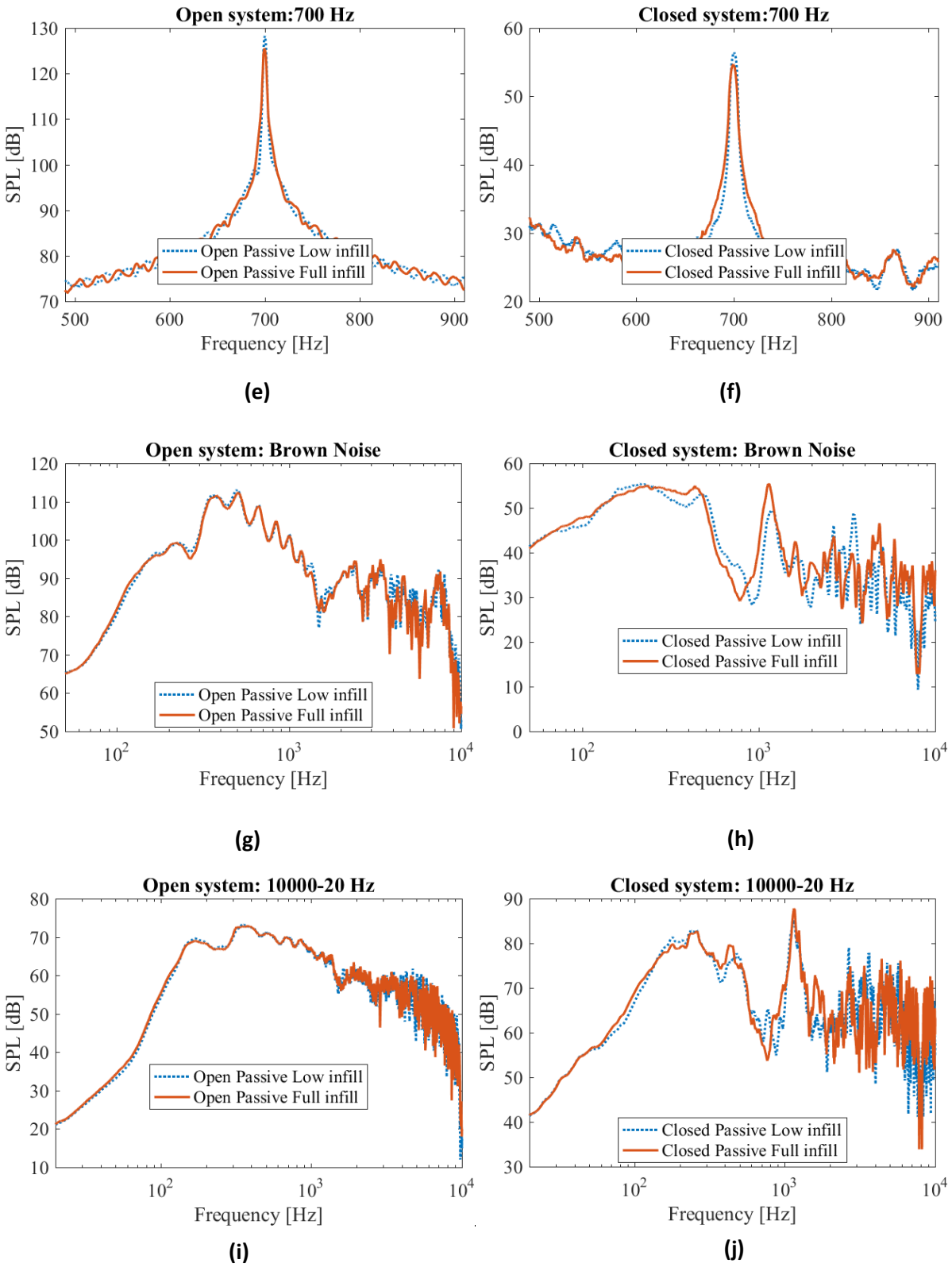

Figure 36: Effect of infill density on the noise attenuation capabilities of the metamaterial

4.2 Pneumatically actuated active metamaterial

The results of the active metamaterial are also subclassified based on the type of actuation and system configuration, i.e., open and closed systems similar to the measurements in the passive metamaterial case. First, the pneumatic actuated case is presented with a few noise samples as compared to the second actuation case because of the limitations of the commercially inflatable balloons.

The pneumatic actuated system, due to the non-uniform response of inflatable balloons to the pressure input, results in a distributed cavity depth in the short and deep regimes. Since the accurate depths from the inflation of the balloons could not be determined, a random distribution of depths is assumed. The number of tests that were conducted using this approach is limited as the fatigue performance of commercially available inflatable balloons is significantly low, allowing for a reduced number of actuations of the resonator cavity depth. The results of these samples are presented in this section.

4.2.1 Open system

From the open system measurements, the difference in performance between the two positions of the ends is noticed to be subtle. The system with larger cavity depths (i.e. 0.05 bar) tend to perform better at lower frequencies, while the system with smaller cavity depths (i.e. 0.15 bar) performs better towards the higher end of the spectrum, but nearly up to 1kHz as shown in Figure 37. This is not an unexpected performance since according to the Helmholtz resonance equation (1), the volume of the resonator cavity is inversely proportional to the resonant frequency. Furthermore, from Figure 37 it can be noticed that the white noise attenuation response of the metamaterial between 0 and 150 Hz at a pressure of 0.05 bar is significantly higher as compared to the other plots. This outlying behavior can only be explained as a measurement anomaly as this type of response is not seen in any of the prior cases tested.

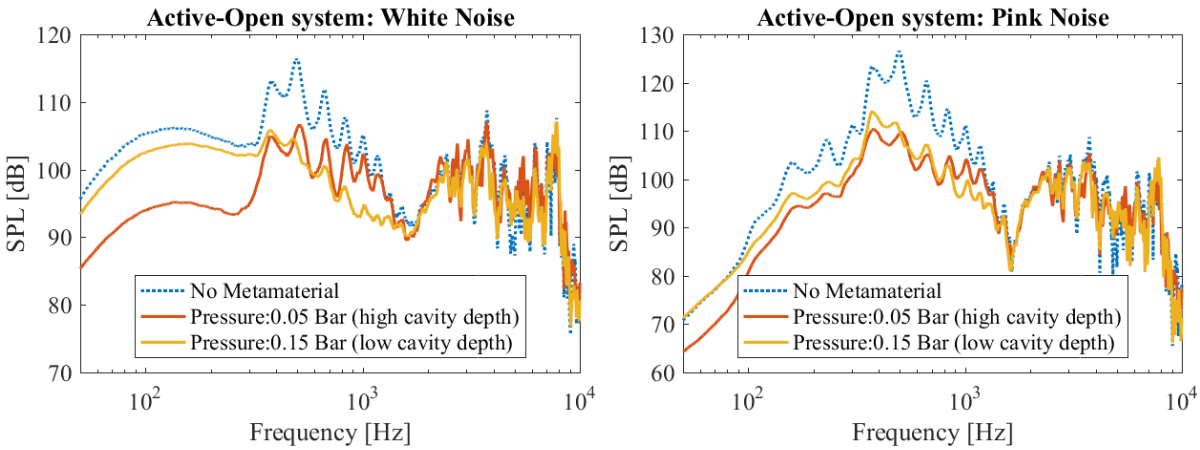

(a) **(b)**

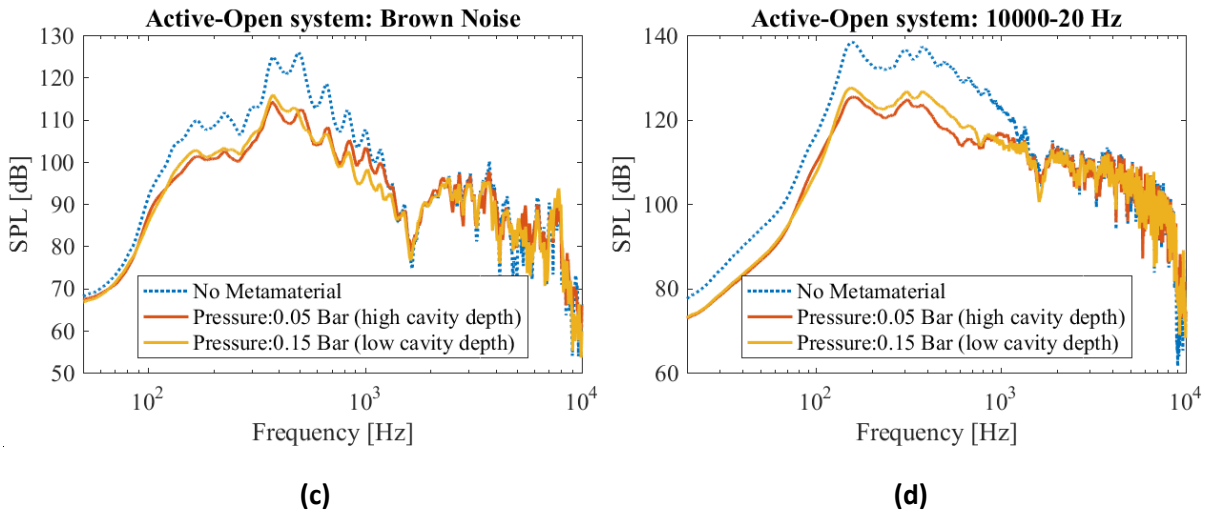

Figure 37: Measured noise levels in the open system experimental case for (a) white noise (b) pink noise (c) brown noise and (d) frequency sweep from 10000 to 20 Hz comparing the performance for two pressure levels (0.05 bar and 0.15 bar)

4.2.2 Closed system

The closed system measurements, unlike the open system, shows more distinct regions of performance. From the plots in Figure 38, it is clearly observed that a higher pressure level (i.e. smaller cavities) accounts to attenuation in a higher frequency range. For example with the white noise sample, the lower pressure pertaining to a higher cavity depth performs better at frequencies below 200 Hz. Although the previously explained effect of closed system noise attenuation can explain the higher degree of sound-pressure-level reduction, the regions of isolated effect establish the performance of the metamaterial.

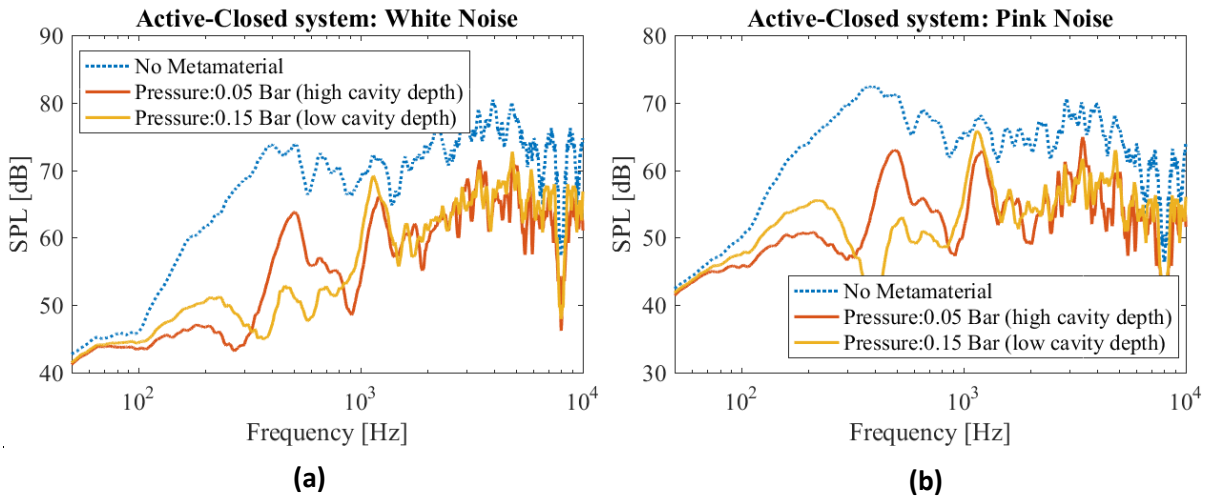

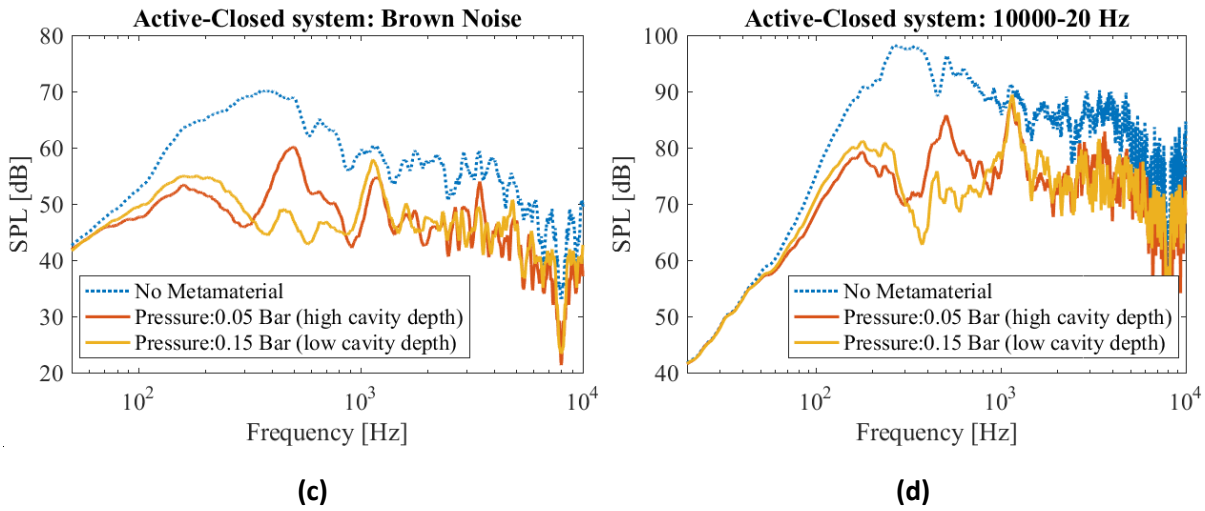

Figure 38: : Measured noise levels in the closed system experimental case for (a) white noise (b) pink noise (c) brown noise and (d) frequency sweep from 10000 to 20 Hz

4.3 Electric actuated active metamaterial

The electromagnetic actuation provides for the possibility of altering dimensions of a large number of resonators in a combined fashion. This allows a more concentrated testing area to prove the effects of the concept at hand. The system was tested with a multitude of sample frequencies, as it does not work with the restrictions of multiple actuations as seen in the pneumatic actuation case. Similar to the other presented cases, electric actuated metamaterial also was tested in open and a closed system setups. In the results shown, a comparison between the different cavity depths tested has been presented to give an idea of the performance of the metamaterial at different frequencies. Finally, the results from the frequency measurements are compared with that of the theoretical results to obtain the precision of the metamaterial at different cavity depths.

4.3.1 Open system

The open system tests show that there are reasonably narrow bands of frequencies that are attenuated at the corresponding resonant frequencies for the selected cavity depths as seen in Figure 40. For instance, in the plot with the pink noise sample, clear dips can be seen at around 190 Hz for 50 mm depth, 210 Hz for 40 mm depth, 235 Hz for 30 mm, 305 Hz for 20 mm and 500 Hz for 10 mm. Similar frequency dips can be seen in the plots of the white and brown noise samples. These bands being narrow tend to not appear in the tests of most isolated noise samples. However can be clearly identified in the plots of white, pink and brown noise. This implies that since the readings are taken at a 50 Hz interval, if the target frequency of a particular fixed cavity depth lies in between two frequency bands that do not overlap, the maximal effect of the attenuation might not appear in the single frequency measurements before or after the target frequency but are prominently seen in the white noise and the frequency sweep test samples. This can be visualized through an example. If a certain tolerance for the neck diameter and the cavity depth is considered, a corresponding net error in the target frequency can be observed. This is theoretically obtained from the Helmholtz equation. For instance, if a target frequency of 125 Hz were chosen, the region of performance would be between

110 Hz to 140 Hz. Since the noise samples tested for are spaced at 50 Hz, this accounts to 100 Hz and 150 Hz test samples. Here, since the region of performance of the metamaterial does not overlap with the test frequencies, the attenuation effect due to the current cavity depth might not be observed with these tests. This effect due to the margin of error is represented by Figure 39. This effect is seen prominently in the closed system attenuation plot Figure 46 where the curve corresponding to a cavity depth of 50 mm (green curve) does not show significant attenuation peaks in the frequency range. The metamaterial with this cavity depth was ideally designed to perform at around 180 Hz but since this is not within the measured sample frequencies, the attenuation effect is not shown.

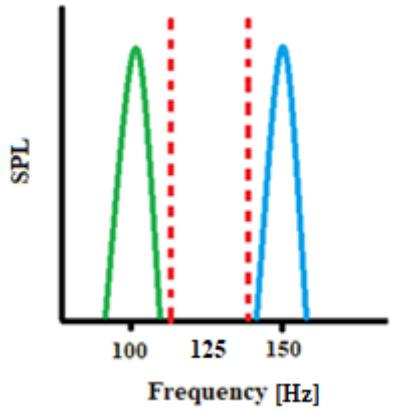

Figure 39: Schematic plot describing the region of performance in untested sample space for a fixed resonator depth. The area enclosed by the red dotted lines represents the metamaterial performance margin for the fixed cavity depth

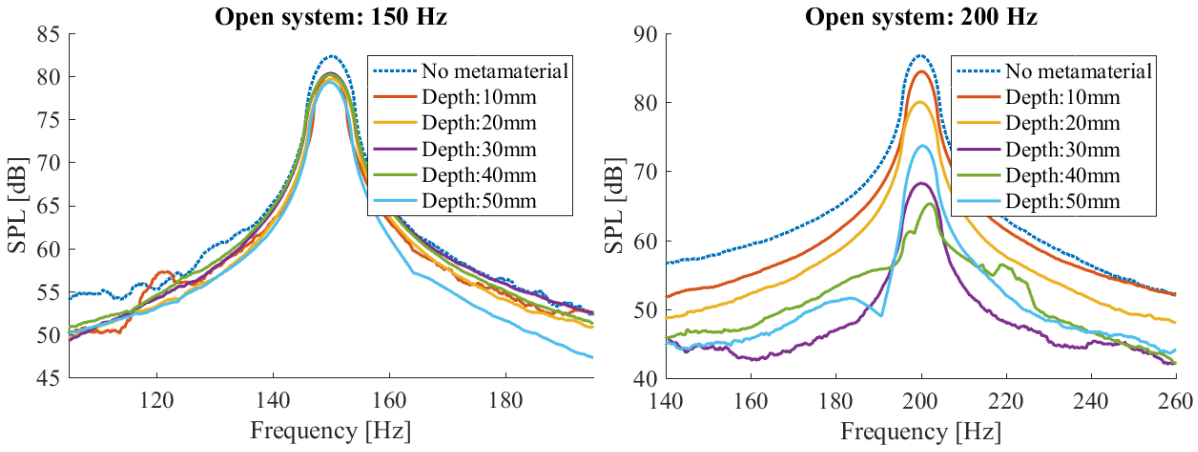

(a) **(b)**

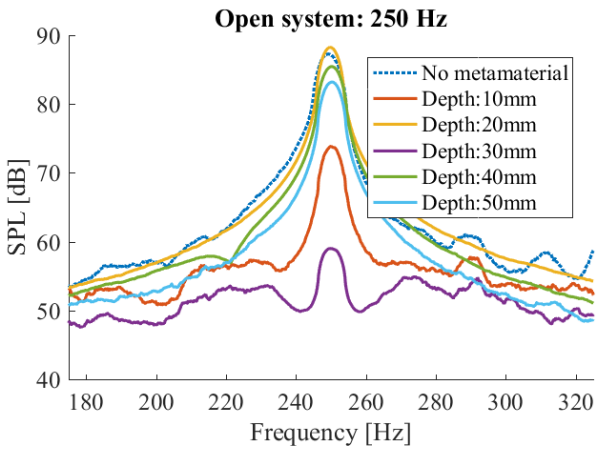
Open system: 250 Hz
SPL [dB]
Frequency [Hz]
No metamaterial
Depth:10mm
Depth:20mm
Depth:30mm
Depth:40mm
Depth:50mm

(c)

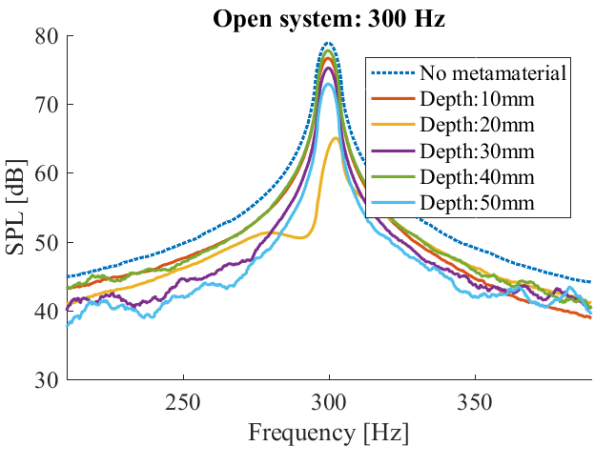
Open system: 300 Hz
SPL [dB]
Frequency [Hz]
No metamaterial
Depth:10mm
Depth:20mm
Depth:30mm
Depth:40mm
Depth:50mm

(d)

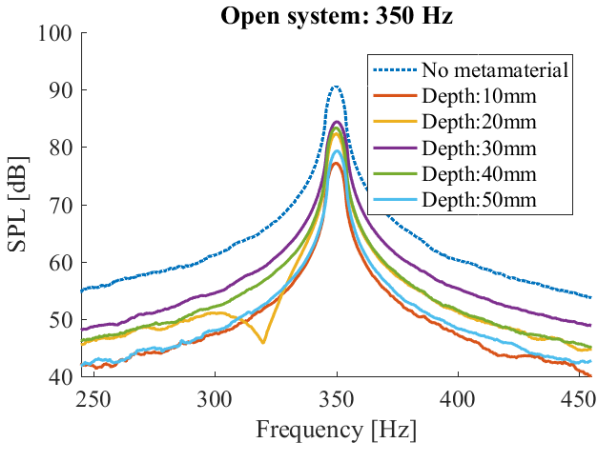
Open system: 350 Hz
SPL [dB]
Frequency [Hz]
No metamaterial
Depth:10mm
Depth:20mm
Depth:30mm
Depth:40mm
Depth:50mm

(e)

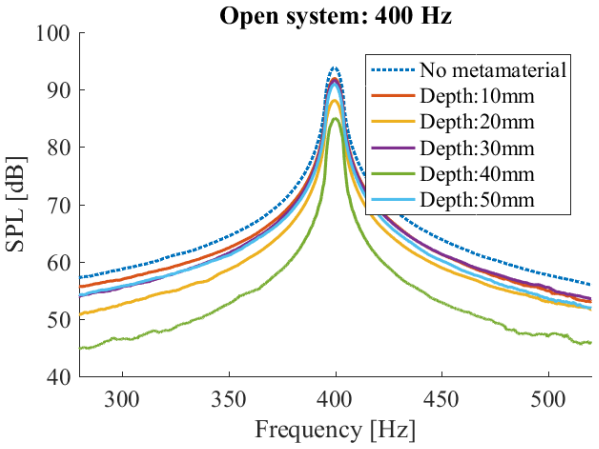
Open system: 400 Hz
SPL [dB]
Frequency [Hz]
No metamaterial
Depth:10mm
Depth:20mm
Depth:30mm
Depth:40mm
Depth:50mm

(f)

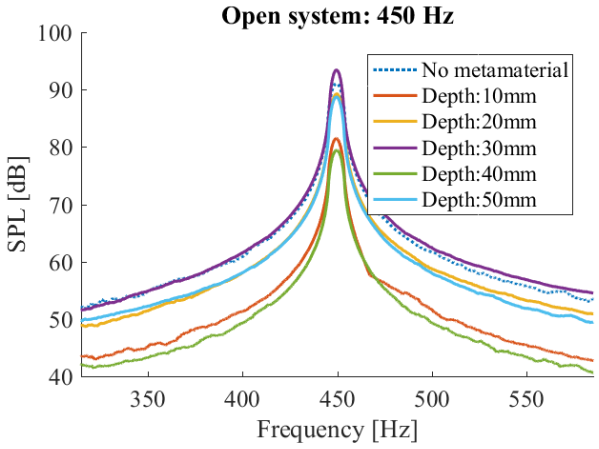
Open system: 450 Hz
SPL [dB]
Frequency [Hz]
No metamaterial
Depth:10mm
Depth:20mm
Depth:30mm
Depth:40mm
Depth:50mm

(g)

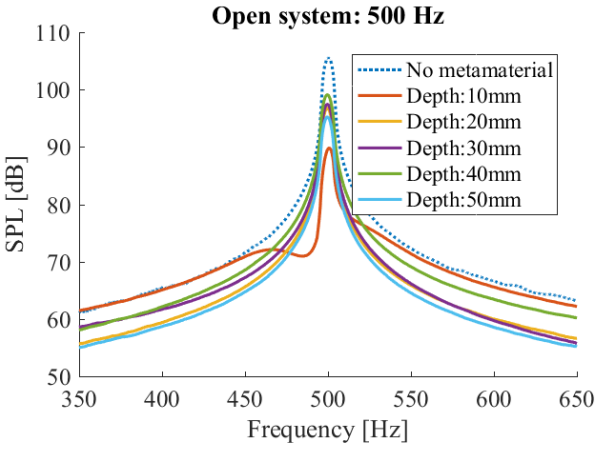
Open system: 500 Hz
SPL [dB]
Frequency [Hz]
No metamaterial
Depth:10mm
Depth:20mm
Depth:30mm
Depth:40mm
Depth:50mm

(h)

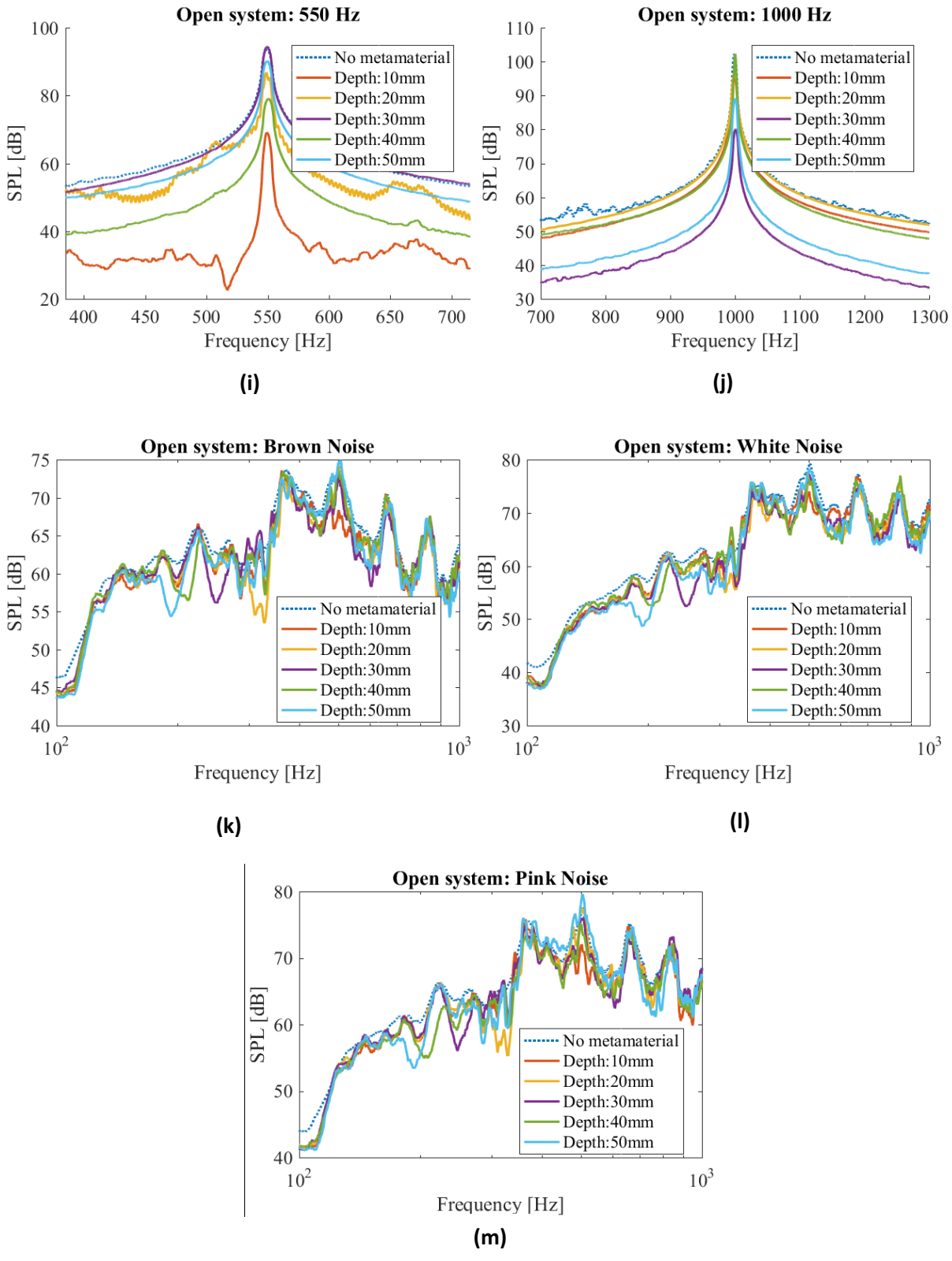

Figure 40: Noise amplitude measurements for the open system for different isolated frequencies and white, pink and brown noise samples. Reliable results may be observed from (l), (m) and (n) because of the error factors explained previously

From the results of the individual frequencies, a difference between the calculated and measured frequencies is drawn to determine the precision of the metamaterial. From Table 5 it can be observed

that the theoretical and the measured values mostly agree and have a maximum difference of 21 Hz. Figure 41 representing the measured and targeted attenuation performances also shows the agreement of the experimental values with the calculated target frequencies for different cavity depths. Furthermore, the attenuation performances of each cavity depth corresponding to different isolated frequencies are compared (Figure 42). The vertical lines represent the target frequencies for each corresponding cavity depth thus showing the deviation of the peaks from the targeted frequencies which is also listed in Table 5. The maximum attenuation peak of each curve can be seen significantly at the corresponding targeted frequency. For example, the 30 mm cavity depth curve shows maximum attenuation at around 250 Hz which is also seen in Figure 40c. It can also be noticed from Figure 42 that the magnitude of the attenuation peaks are different from those seen in the brown, pink and white noise samples (Figure 40k,l,m) . This behavior of producing a higher level of attenuation while testing for isolated frequencies as compared to large frequency bands is seen to be consistent in all cases tested. However, the reasons for this behavior cannot be speculated with the tests conducted thus far.

Table 5: Comparison of calculated and experimental frequencies describing the obtained precision of the metamaterial (as obtained from the closed system)

Cavity Depth [mm]	Target frequency [Hz]	Obtained frequency [Hz]	Error [%]
10	507	500	1.4
20	318	305	4.1
30	251	230	8.4
40	214	205	4.2
50	189	200	5.8

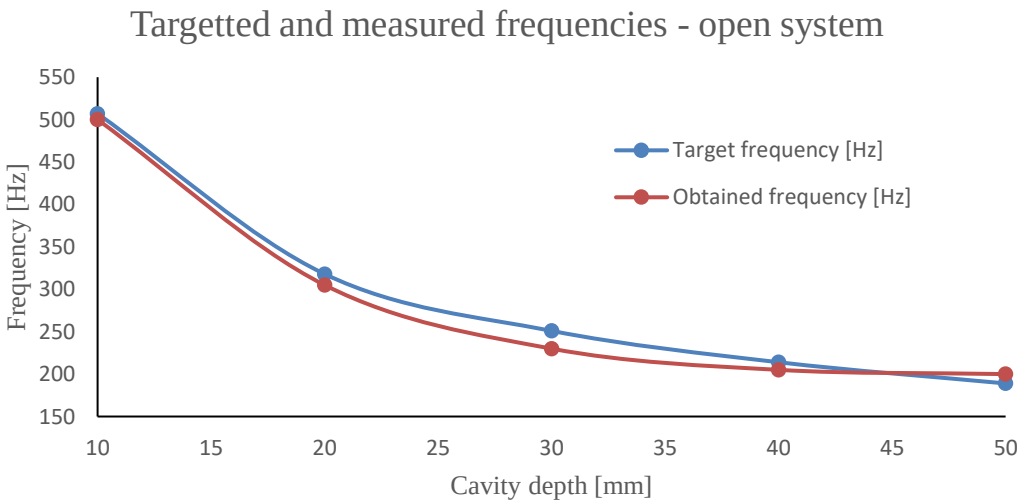

Figure 41: Comparison of attenuation performance of the open system with targeted and measured frequencies for different cavity depths

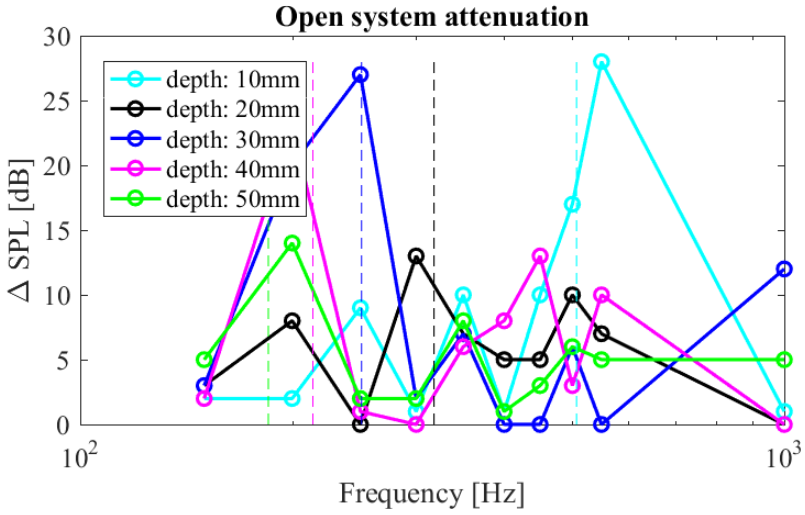

Figure 42: Open system attenuation at different frequencies for different cavity heights. Theoretical target frequencies are demonstrated by vertical dashed lines.

4.3.2 Closed system

Similar to the previous closed system cases, the closed system effect is seen consistent with this case as seen in Figure 43. The sound attenuation corresponding to the resonators is nearly comparable to the open system. As seen in white, pink and brown noise measurements, clear dips in the attenuation levels can be observed at corresponding frequencies. In the brown noise plot, the attenuation performance of different cavity depths can be seen at approximately 500 Hz for 10 mm, 310 Hz for 20 mm, 220 Hz for 30 mm, 205 Hz for 40 mm and 180 Hz for 50 mm. Similar trends can be noticed for the white and pink noise samples as well.

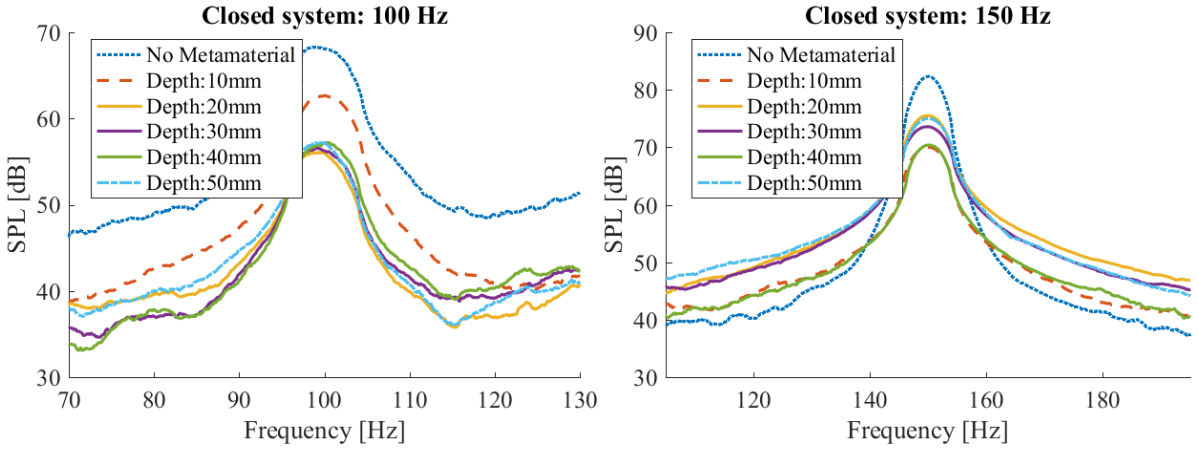

(a) **(b)**

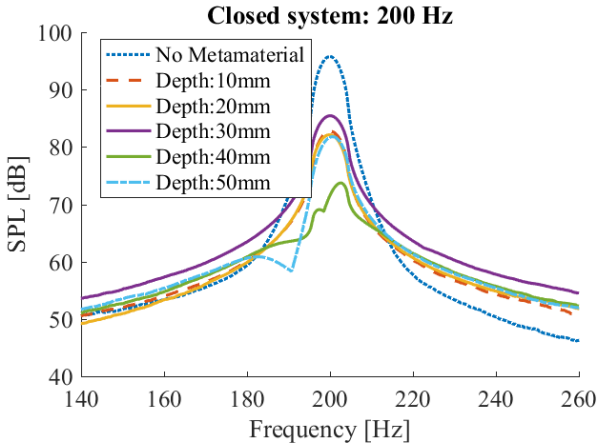
Closed system: 200 Hz
No Metamaterial
Depth:10mm
Depth:20mm
Depth:30mm
Depth:40mm
Depth:50mm
SPL [dB]
Frequency [Hz]

(c)

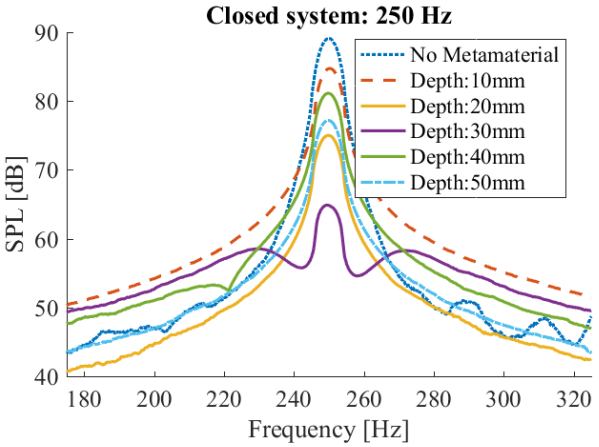
Closed system: 250 Hz
No Metamaterial
Depth:10mm
Depth:20mm
Depth:30mm
Depth:40mm
Depth:50mm
SPL [dB]
Frequency [Hz]

(d)

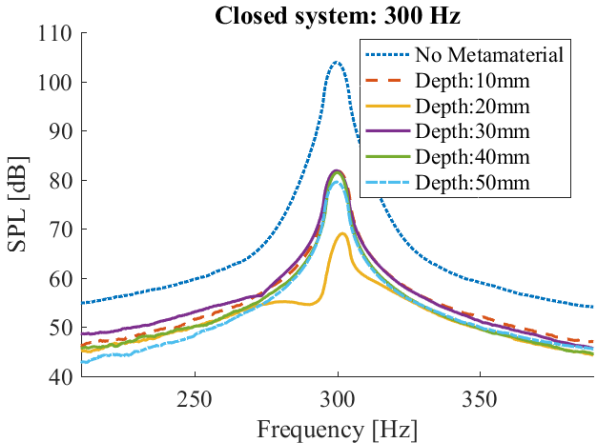
Closed system: 300 Hz
No Metamaterial
Depth:10mm
Depth:20mm
Depth:30mm
Depth:40mm
Depth:50mm
SPL [dB]
Frequency [Hz]

(e)

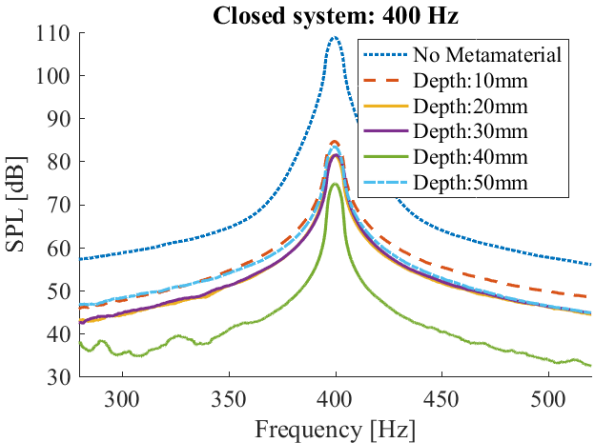
Closed system: 400 Hz
No Metamaterial
Depth:10mm
Depth:20mm
Depth:30mm
Depth:40mm
Depth:50mm
SPL [dB]
Frequency [Hz]

(f)

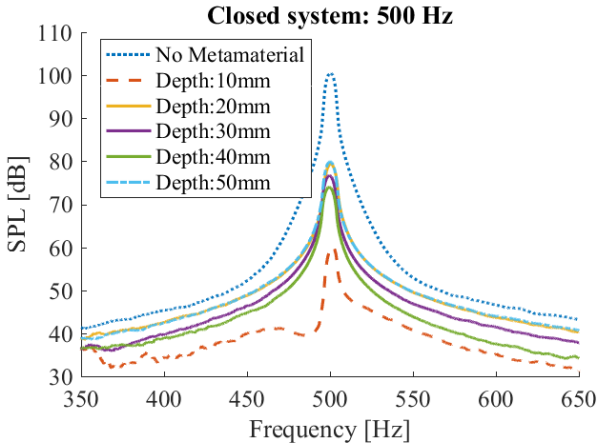
Closed system: 500 Hz
No Metamaterial
Depth:10mm
Depth:20mm
Depth:30mm
Depth:40mm
Depth:50mm
SPL [dB]
Frequency [Hz]

(g)

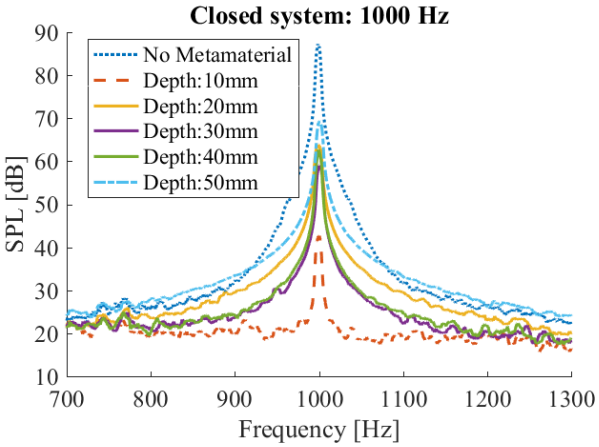
Closed system: 1000 Hz
No Metamaterial
Depth:10mm
Depth:20mm
Depth:30mm
Depth:40mm
Depth:50mm
SPL [dB]
Frequency [Hz]

(h)

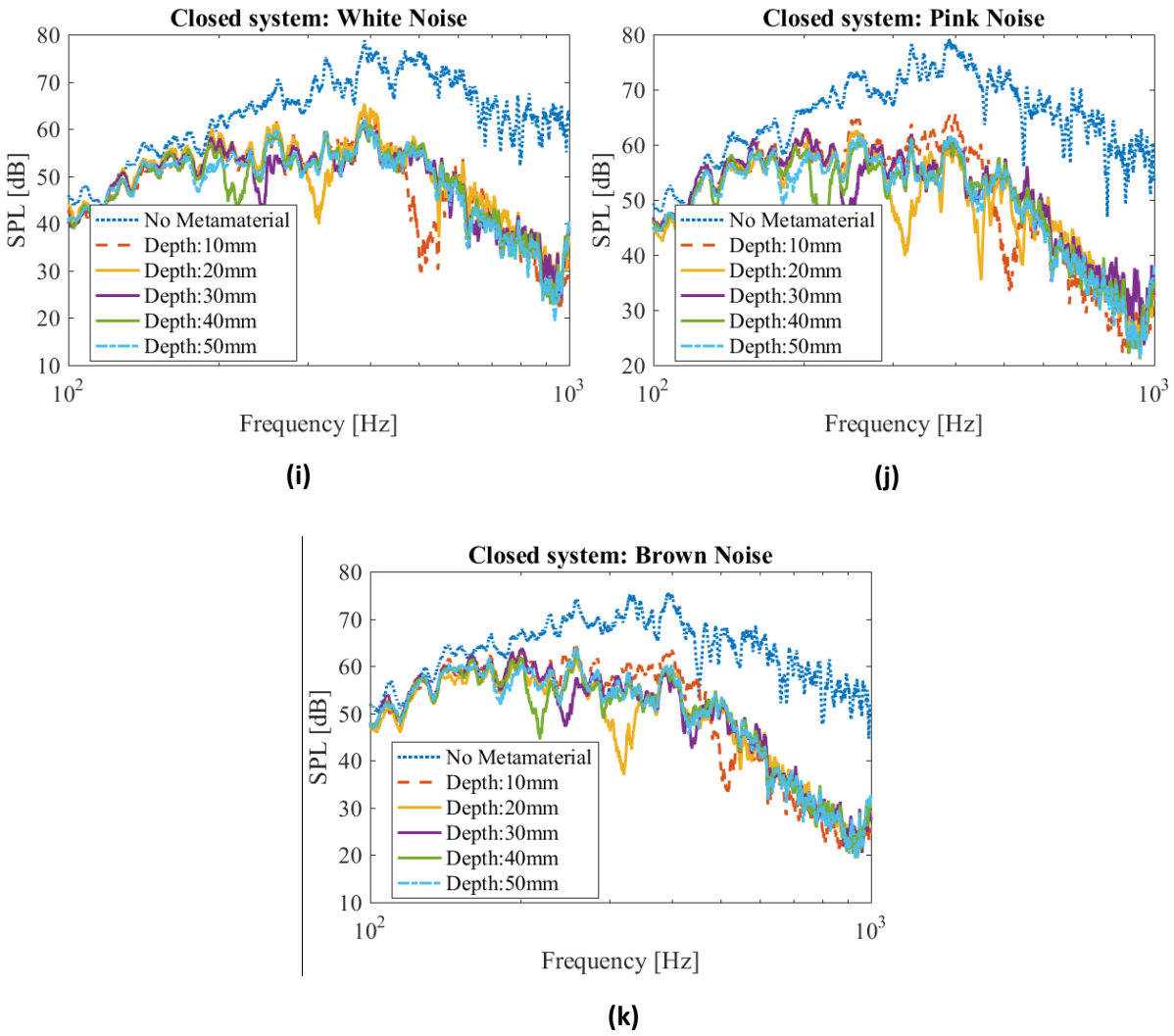

Figure 43: Noise amplitude measurements for the closed system for different isolated frequencies and white, pink and brown noise samples

To prove that the system can be used for different frequencies simultaneously, the depths of the resonator cavities are kept at 10mm and 50mm on three and two walls respectively. The results of this test as seen in Figure 44 suggest that the metamaterial is capable of targeting multiple frequencies. In this graph, clear peaks are seen at 190 Hz and 500 Hz. However, the amplitude of attenuation reduces as compared to a single cavity depth for all metamaterial walls, targeting a single frequency.

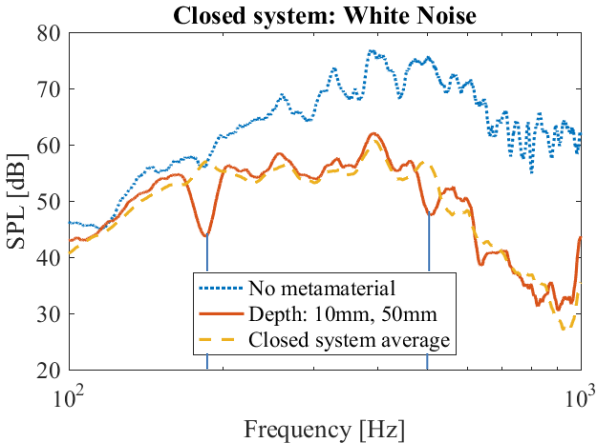

Figure 44: Amplitude measurement showing two simultaneous dips for frequencies at around 190 Hz and 500 Hz

Table 6 shows the comparison of the targeted or design frequencies with the obtained frequencies. Similar to the open system, the closed system measurements also seem to agree with the calculates target frequencies. The maximum deviation between the target and obtained frequencies accounts to 17 Hz, which represents a fairly good precision of the metamaterial (Figure 45). The attenuation performance of the closed system compiled from the isolated frequency performance tests can be seen in Figure 46. The vertical lines represent the target frequencies for each corresponding cavity depth. The attenuation performance here is to be read from the meanline performance of the metamaterial to identify zones of resonator-targeted attenuation. The meanline performance highlights the closed system effect as explained in section 4.1.2. It can be seen that the metamaterial provides an attenuation of 15 dB over the meanline performance at frequencies corresponding to each cavity depth. For example, the metamaterial at a cavity depth of 40 mm provides an attenuation of 12 dB over the meanline attenuation of 13 dB at 200 Hz, which can also be seen in Figure 44c and Figure 44j. Similar to the open system, this plot also shows the magnitude of attenuation greater than that in the white, pink and brown noise plots for the same reason as explained in section 4.3.1.

Table 6: Comparison of experimental and calculated frequency measurements showing the obtained precision of the metamaterial (as obtained from the closed system)

Cavity Depth [mm]	Target frequency [Hz]	Obtained frequency [Hz]	Error [%]
10	507	490	3.4
20	318	307	3.5
30	251	235	6.4
40	214	202	5.6
50	189	180	4.8

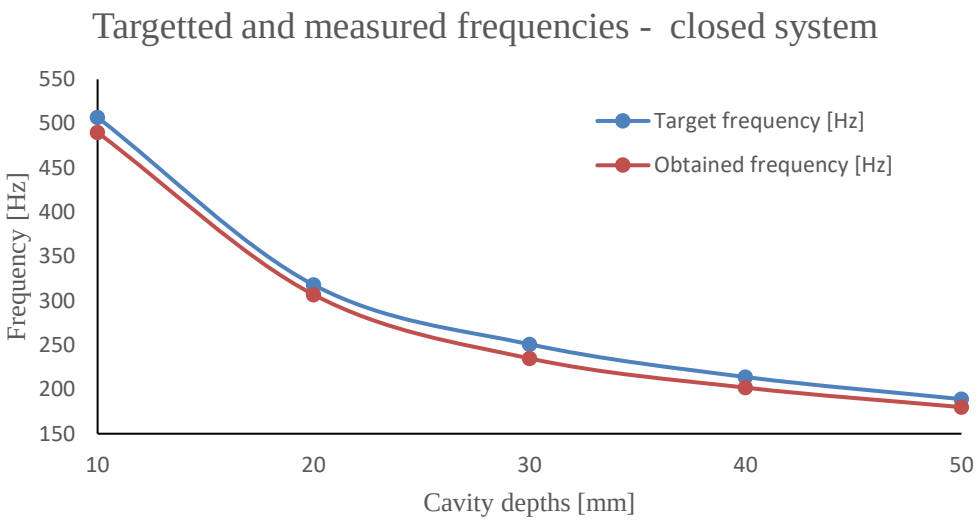

Figure 45: Comparison of attenuation performance of the closed system with targeted and measured frequencies for different cavity depths

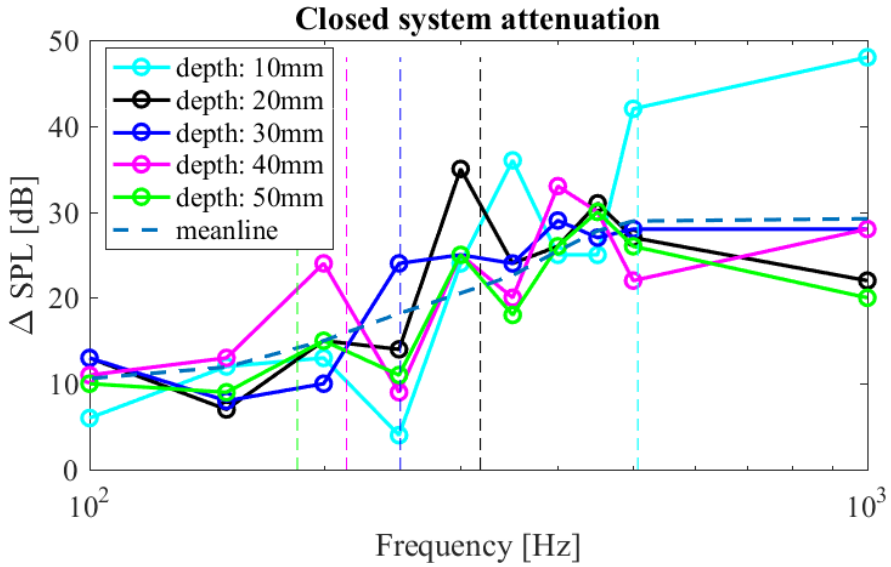

Figure 46: Closed system attenuation at different frequencies for different cavity heights. Theoretical target frequencies are demonstrated by vertical dashed lines.

5

Conclusion

Metamaterials offer a multitude of applications in almost all sectors of the technical world. The ability of materials to modify their properties just based on their structural modifications for catering to various requirements offers a great advantage over the other classes of materials currently being used. Recent advancements in acoustic metamaterials have led way to developments in the field of noise control, which has been a driving need especially in the automotive and aerospace industries that are currently focusing a lot on passenger comfort. Acoustic metamaterials in this aspect provide an immense advantage predominantly since recent developments have led to activation of different parts to attenuate different noise levels. Most recent developments include designs for vibration suppressions in structures using laminate acoustic metamaterials made of carbon fiber reinforced composites (CFRP) [55].

From literature, it is understood that there have been many studies and designs for the purpose of attenuating noise levels. However, acoustic metamaterial designs incorporating Helmholtz resonators has been a fairly new branch of research. Helmholtz resonators are used for its simplistic design and accuracy in frequency targeting. In this report, an improvised design has been presented, with an active system to target a broadband frequency range, as well as a range of isolated frequencies. In line with the set project goals, a passive model has been fabricated with design parameters catering to this frequency range. The passive model consists of four or five walls of an 8x8 matrix of Helmholtz resonator unit cells that are identical in all dimensions, except the cavity depth. This passive model has been tested in an open system consisting of four walls lining the perimeter of a tube path, and a closed system consisting of five walls creating a partial cube system, to identify the performance in closed areas as well as a tube or tunnel system. The unit cell arrangement being random, results in the attenuation region varying based on the configuration of the system. The open system performs best at a frequency of 150 Hz, providing an attenuation of 18 dB. The closed system on the other hand shows its best performance at a frequency of 350 Hz, providing a peak attenuation of 33 dB.

During fabrication, the possibility of reducing the mass of the system presented itself in the form of infill density of the additive manufacturing process. Two models of identical dimensions and varying masses of 430 g and 330 g have been tested. The results of these tests although, hypothesized to be better for higher massed structure, proved to be independent of this design variable. These results however may need additional testing due to the limited number of test sample cases.

Based on the performance of the passive model, an active model was fabricated with similar dimensions. The chosen variable parameter for active modulation was the volume of the resonator cavity through the change of the resonator cavity depth. The depths selected correspond to different resonant frequencies based on the Helmholtz resonance equation. For the actuation method, two mechanisms were selected and tested: a pneumatic actuation and an electric actuation. From the proposed methods of actuation, it was seen that the pneumatic model operates at a wider frequency

range due to the inherent uncertainty of cavity depths due to the use of commercially available balloons as actuators. On the other hand, the electric actuation gives more precision to dimensional change targeted in this design, thereby providing a highly concentrated operational frequency range. The design operational frequency range was chosen to be between 170 Hz to 450 Hz. The depths of the resonators were calculated in order to fit within this range. From the results, it is seen that in the pneumatically actuated model, the region of performance shifts from a frequency range of 150 Hz–350 Hz at higher cavity depths to a frequency range of 300Hz – 600 Hz at a lower cavity depth. The pneumatically actuated system is observed to have a peak attenuation level in the order of 20 dB (at 500 Hz) in the closed system and 15 dB (at 500 Hz) in the open system, though the open system measurements are not observed to be precise due to fabrication and test setup inaccuracies. In the case of the electric actuation, constant depths of the cavities at intervals of 10 mm were tested with. As hypothesized, the different depths yielded dips in the noise level for the corresponding frequencies as seen in the plots for the white, pink and brown noise samples. The accuracy of the system is found to be of the order of ± 20 Hz. This is seen due to the discrepancies in alignment of the cavity bases and in turn their respective position and cavity depths. The attenuation obtained for this model is around 10 dB – 15 dB over the mean line performance, at the corresponding cavity depths for the closed system, and between 15 dB – 20 dB, at corresponding cavity depths for the open system. The closed system was tested for performance at multiple cavity depths by maintaining two walls at 10 mm cavity depth and three walls at 50 mm cavity depth. This test provided for an attenuation of 15 dB at 180 Hz, the frequency corresponding to the 50 mm cavity depth, and 10 dB at 515 Hz, corresponding to the 10 mm cavity depth.

In conclusion, the active system thus designed provides a precise control over the range of the targeted frequencies. Unlike most other studies conducted, this active acoustic design is capable of attenuating isolated frequencies as well as multiple frequencies simultaneously. The active system described here provides attenuation performance comparable results to the passive metamaterial as seen in the pneumatically actuated system. The added control that is achieved through the incorporation of the electric linear motor based actuation allows for the advantage of accurate frequency targeting along with the base attenuation levels of the passive resonant acoustic metamaterial.

References

1. Veselago, V.G., *The electrodynamics of substances with simultaneously negative values of and μ.* Soviet physics uspekhi, 1968. **10**(4): p. 509.
2. Schurig, D., et al., *Metamaterial electromagnetic cloak at microwave frequencies.* Science, 2006. **314**(5801): p. 977-980.
3. Driscoll, T., et al., *Dynamic tuning of an infrared hybrid-metamaterial resonance using vanadium dioxide.* Applied Physics Letters, 2008. **93**(2): p. 024101.
4. Hedayati, R., A.M. Leeflang, and A.A. Zadpoor, *Additively manufactured metallic pentamode meta-materials.* Applied Physics Letters, 2017. **110**(9).
5. Hedayati, R., et al., *Action-at-a-distance metamaterials: Distributed local actuation through far-field global forces.* APL Materials, 2018. **6**(3): p. 036101.
6. Kolken, H.M. and A. Zadpoor, *Auxetic mechanical metamaterials.* RSC Advances, 2017. **7**(9): p. 5111-5129.
7. Esteve, S.J. and M.E. Johnson, *Adaptive Helmholtz resonators and passive vibration absorbers for cylinder interior noise control.* Journal of Sound and Vibration, 2005. **288**(4-5): p. 1105-1130.
8. Liu, Z., et al., *Locally resonant sonic materials.* Science, 2000. **289**(5485): p. 1734-1736.
9. Smith, D.R., et al., *Composite medium with simultaneously negative permeability and permittivity.* Physical review letters, 2000. **84**(18): p. 4184.
10. Li, J. and C. Chan, *Double-negative acoustic metamaterial.* Physical Review E, 2004. **70**(5): p. 055602.
11. Yang, Z., et al., *Membrane-type acoustic metamaterial with negative dynamic mass.* Phys Rev Lett, 2008. **101**(20): p. 204301.
12. Yang, M., et al., *Coupled membranes with doubly negative mass density and bulk modulus.* Physical review letters, 2013. **110**(13): p. 134301.
13. Huang, H., C. Sun, and G. Huang, *On the negative effective mass density in acoustic metamaterials.* International Journal of Engineering Science, 2009. **47**(4): p. 610-617.
14. Langfeldt, F., et al., *Perforated membrane-type acoustic metamaterials.* Physics Letters A, 2017. **381**(16): p. 1457-1462.
15. Chen, H., et al., *Double-negative acoustic metamaterial based on hollow steel tube meta-atom.* Journal of Applied Physics, 2013. **113**(10): p. 104902.
16. Chen, Y., et al., *Analytical coupled vibroacoustic modeling of membrane-type acoustic metamaterials: Membrane model.* The Journal of the Acoustical Society of America, 2014. **136**(3): p. 969-979.
17. Lu, K., et al., *A lightweight low-frequency sound insulation membrane-type acoustic metamaterial.* AIP Advances, 2016. **6**(2).
18. Ma, F. and J.H. Wu, *PLATE-TYPE ACOUSTIC METAMATERIALS.*
19. Badreddine Assouar, M., et al., *Broadband plate-type acoustic metamaterial for low-frequency sound attenuation.* Applied Physics Letters, 2012. **101**(17): p. 173505.
20. Liang, Z. and J. Li, *Extreme acoustic metamaterial by coiling up space.* Physical review letters, 2012. **108**(11): p. 114301.
21. Li, Y., et al., *Acoustic focusing by coiling up space.* Applied Physics Letters, 2012. **101**(23): p. 233508.
22. Ghaffarivardavagh, R., et al., *Horn-like space-coiling metamaterials toward simultaneous phase and amplitude modulation.* Nature communications, 2018. **9**(1): p. 1349.
23. Krushynska, A.O., F. Bosia, and N.M. Pugno, *Labyrinthine acoustic metamaterials with space-coiling channels for low-frequency sound control.* Acta Acustica united with Acustica, 2018. **104**(2): p. 200-210.

24. Liang, Z., et al., *Space-coiling metamaterials with double negativity and conical dispersion.* Scientific reports, 2013. **3**: p. 1614.
25. Norris, A.N. *Acoustic cloaking theory*. in *Proceedings of the Royal Society of London A: Mathematical, Physical and Engineering Sciences*. 2008. The Royal Society.
26. Zigoneanu, L., B.-I. Popa, and S.A. Cummer, *Three-dimensional broadband omnidirectional acoustic ground cloak.* Nature materials, 2014. **13**(4): p. 352.
27. Zhang, S., C. Xia, and N. Fang, *Broadband acoustic cloak for ultrasound waves.* Physical Review Letters, 2011. **106**(2): p. 024301.
28. Kan, W., et al., *Broadband acoustic cloaking within an arbitrary hard cavity.* Physical Review Applied, 2015. **3**(6): p. 064019.
29. Sui, N., et al., *A lightweight yet sound-proof honeycomb acoustic metamaterial.* Applied Physics Letters, 2015. **106**(17).
30. Claeys, C., et al., *A lightweight vibro-acoustic metamaterial demonstrator: Numerical and experimental investigation.* Mechanical Systems and Signal Processing, 2016. **70-71**: p. 853-880.
31. Yang, X.W., J.S. Lee, and Y.Y. Kim, *Effective mass density based topology optimization of locally resonant acoustic metamaterials for bandgap maximization.* Journal of Sound and Vibration, 2016. **383**: p. 89-107.
32. Wolfe, J., *Helmholtz resonance.* School of Physics at UNSW, Sydney, Australia: http://www. phys. unsw. edu. au/jw/Helmholtz. html (2013/1/20), 2000.
33. Groby, J.-P., et al., *Enhancing the absorption properties of acoustic porous plates by periodically embedding Helmholtz resonators.* The Journal of the Acoustical Society of America, 2015. **137**(1): p. 273-280.
34. Ding, C.-L. and X.-P. Zhao, *Multi-band and broadband acoustic metamaterial with resonant structures.* Journal of Physics D: Applied Physics, 2011. **44**(21): p. 215402.
35. Wu, D., et al., *Noise Attenuation Performance of a Helmholtz Resonator Array Consist of Several Periodic Parts.* Sensors, 2017. **17**(5): p. 1029.
36. Zhao, D., et al., *Acoustic damping of a Helmholtz resonator with an oscillating volume.* AIAA journal, 2009. **47**(7): p. 1672-1679.
37. Anwar, A., *Low frequency finite element modeling of passive noise attenuation in ear defenders*. 2005, Virginia Tech.
38. Sacarcelik, O., *Acoustic devices for the active & passive control of sound in a payload compartment*. 2004, Virginia Tech.
39. Birdsong, C. and C.J. Radcliffe, *An electronically tunable resonator for noise control.* Mechanical Engineering, 2001: p. 28.
40. De Bedout, J.M., et al., *Adaptive-passive noise control with self-tuning Helmholtz resonators.* Journal of Sound and Vibration, 1997. **202**(1): p. 109-123.
41. Nagaya, K., Y. Hano, and A. Suda, *Silencer consisting of two-stage Helmholtz resonator with auto-tuning control.* the Journal of the Acoustical Society of America, 2001. **110**(1): p. 289-295.
42. Cheer, J., C. McCormick, and S. Daley, *An active acoustic metamaterial for the control of sound transmission.* 2016.
43. Kela, L., *Adaptive Helmholtz resonator in a hydraulic system.* World Academy of Science, Engineering and Technology, 2010. **44**: p. 1002-1009.
44. Yuan, J., *Active Helmholtz resonator with positive real impedance.* Journal of vibration and acoustics, 2007. **129**(1): p. 94-100.
45. Singh, S., C. Howard, and C. Hansen. *Tuning a semi-active Helmholtz resonator*. in *6th International Symposium on Active Noise and Vibration Control (ACTIVE 2006), Adelaide, Australia, September*. 2006.
46. Kela, L., *Resonant frequency of an adjustable Helmholtz resonator in a hydraulic system.* Archive of Applied Mechanics, 2009. **79**(12): p. 1115-1125.

47. Matsuhisa, H., B. Ren, and S. Sato, *Semiactive control of duct noise by a volume-variable resonator.* JSME international journal. Ser. 3, Vibration, control engineering, engineering for industry, 1992. **35**(2): p. 223-228.
48. Jollivet, T., et al., *Rapid manufacturing of polymer parts by selective laser sintering.* International Journal of Material Forming, 2009. **2**(1): p. 697.
49. Gibson, I. and D. Shi, *Material properties and fabrication parameters in selective laser sintering process.* Rapid Prototyping Journal, 1997. **3**(4): p. 129-136.
50. Mohamed, O.A., S.H. Masood, and J.L. Bhowmik, *Optimization of fused deposition modeling process parameters: a review of current research and future prospects.* Advances in Manufacturing, 2015. **3**(1): p. 42-53.
51. Prajapati, D., S. Nandwana, and V. Aggarwal, *Fused Deposition Modelling.*
52. Hiemenz, J., *3D printing with FDM: How it Works.* Stratasys Inc, 2011. **1**: p. 1-5.
53. *Fused Deposition Modelling*. Available from: https://www.custompartnet.com/wu/fused-deposition-modeling.
54. Herrmann, B., 2018.
55. He, Z., X. Xiao, and E. Li, *Design for structural vibration suppression in laminate acoustic metamaterials.* Composites Part B: Engineering, 2017. **131**: p. 237-252.